High-Order Accurate Methods in Time-Domain Computational Electromagnetics

A Review

J.S. Hesthaven

Division of Applied Mathematics, Brown University, Box F, Providence, RI 02912, USA

E-mail: Jan.Hesthaven@brown.edu

We present a review of recent efforts to develop high-order accurate methods for the time-domain solution of Maxwell's equations. An emphasis is placed on methods with the potential to address geometrically complex applications, including various incarnations high-order finite difference methods, spectral and spectral multidomain methods, finite volume methods, and continuous and discontinuous finite element formulations. We also discuss temporal integration and discrete stability, and point out important outstanding problems.

Throughout, we attempt to emphasize strengths and limitations of existing methods as well as interesting alternatives. Select examples illustrate the performance of some of the schemes for pure scattering problems, interior problems and problems containing materials.

Key Words: High-Order Accuracy, Maxwell's Equations; Finite Difference Methods; Finite Volume Methods; Finite Element Methods; Discontinuous Galerkin Methods; Spectral Methods; Spectral Multidomain Methods; Time Integration; Structured Grids; Unstructured Grids

CONTENTS

1. INTRODUCTION

The genius of James Clerk Maxwell led to a simple system of equations, known to us as Maxwell's equations, describing the propagation of electromagnetic waves and, combined with constitutive relations and boundary conditions, the interaction of electromagnetic energy with matter. As simple as these equations appear, their importance is tremendous and accurate, efficient, and robust methods for solving them are at the heart of the modeling and design of emerging technologies such as very low observable vehicles, ground/foliage penetrating radars, phase sensitive components, and high-speed electronics and electrooptics.

The simplicity of Maxwell's equations is indeed deceptive and solving them accurately and efficiently in realistic applications remains a significant challenge which continues to attract attention among computational mathematicians, physicists, and engineers alike. What complicates the solution of Maxwell's equations is the need to accurately model the wave-matter interaction, i.e., reflection, refraction, and diffraction processes, the vectorial nature of the boundary conditions, and the size and geometric complexity one often encounters in applications. This imposes requirements on the accuracy and performance of the computational tools well beyond that of existing standard techniques. The need to identify new approaches to electromagnetic modeling and design is further emphasized by the growing interest in very broad band signals and their interaction with large and geometrically complex objects, often involving regions of inhomogeneous, anisotropic, lossy, or even nonlinear materials. Additional complications often involve random surfaces and materials which become of increasing importace as the frequency of the waves increase in applications as and in modeling efforts.

The classical integral based solution techniques [17], as unchallenged as they are for pure scattering problems, are less appealing for broadband applications and problems including penetration, complex materials, and random effects. Finite element techniques [69, 120] can, at significant cost, successfully address some of these concerns but does so assuming monochromatic waves. This suggests that one turns the attention to time-domain methods for solving Maxwell's equations. Indeed, the strength of this approach has been successfully demonstrated over the last few decades, beginning with the 2nd order accurate Yee scheme [132]. As simple as this scheme is, it continues to be the main workhorse of computational electromagnetics in the time-domain [116, 117].

It is easy to identify several reasons for the success of the Yee scheme but its most appealing quality is perhaps its simplicity. Furthermore, the use of the staggered grid improves the accuracy somewhat and can be shown to ensure that the divergence of the initial conditions in homogeneous regions is preserved exactly in agreement with Maxwell's equations [132].

The limitations of the Yee scheme are, however, equally straightforward to identify. Apart from the 2nd order accuracy, limiting the electric size and duration of problems one can consider, the embedding of the computational geometry poses the most significant problem by requiring one to approximate boundaries and interfaces by a staircased curve. While this may seem adequate for many problems it nevertheless affects the overall accuracy and essentially reduces accuracy of the scheme to first order. Techniques for overcoming this are plentiful in the literature, see e.g.

[70, 91, 116, 133, 59]. Most of these methods, however, sacrifice the simplicity of the original Yee scheme to achieve the improved accuracy which remains, at best, second order.

However, as the problems increase in size and the geometries in complexity, one begins to encounter the limits of the second order scheme. In particular the accumulating dispersion errors becomes a major concern, see, e.g., [104]. Ways to overcome this problem are, however, few and well known – decrease the grid size or increase the order of the scheme. As the former quickly becomes impractical for large scale problems it is only natural to turn the attention to the development of high-order accurate methods for solving Maxwell's equations in the time-domain. As we shall discuss in Sec. 3, high-order methods are characterized by being able to accurately represent wave propagation over very long distances, using only a few points per wavelength. For three-dimensional large scale computations, this translates into dramatic reductions in the required computational resources, i.e., memory and execution time, and promises to offer the ability to model problems of a realistic complexity and size.

This comes at a price, however. The simplicity of the schemes is sacrificed somewhat for the accuracy, in particular when combined with a need for geometric flexibility. This increased complexity of the scheme is perhaps the main reason for the rather slow acceptance of high-order methods among practitioners of computational electromagnetics. Although the need for high-order accurate schemes was realized by some practitioners early on [92], acceptance of this is still far from wide spread. Evidence of this is the lack of contributions discussing high-order time-domain methods in recent overviews of state-of-the-art techniques in computational electromagnetics [41, 83].

It is the purpose of this review to rectify this by offering an overview of a number of recent efforts directed towards the development of high-order accurate methods for the time-domain solution of Maxwell's equation. By high-order we shall refer to methods with a spatial convergence rate exceeding two. The question of which order of accuracy is suitable for large scale applications is an interesting question in itself and can be analyzed as a cost-benefit question [30, 124, 39]. While the answer naturally has some problem dependence, the general conclusion is that schemes of spatial order four to six offers an optimal balance between accuracy and computational work for a large class of applications. It is therefore natural to focus on methods that have the potential to reach this level of accuracy.

Unavoidably, the discussion is colored by our own interests and experiences and some smaller current developments have not been included in this discussion, most notably perhaps multi-resolution time-domain methods [117]. These methods do display high-order accuracy under certain circumstances, but are notoriously difficult to use for geometrically complex problems. As this remains one of the major concerns, we have chosen not to include a discussion in this review. A good starting point for such methods is [117].

While more selective overviews are available [117, 19] we shall strive to bring most current efforts into the discussion. We hope this, one on hand, will be helpful as a starting point to the practitioner seeking alternatives to standard techniques and, on the other hand, can serve as a updated review of an emerging and rapidly evolving field to the interested computational mathematician.

What remains of this review is organized as follows. In Sec. 2 we recall Maxwell's equations in the time-domain, discuss boundary conditions, various simplifications, and standard normalizations. Section 3 is devoted to an overview of the by now classical phase-error analysis as a way of motivating the need to consider high-order accurate methods in time-domain electromagnetics, in particular as problems increase in size and complexity. This sets the stage for Sec. 4 where we discuss extensions of the Yee scheme and other more complex finite difference schemes. It will become apparent that a major challenge in the development of high-order methods is in fact not to achieve the high order accuracy but rather to do this in ways that enables geometric flexibility. An interesting development in this direction is the emerging embedding techniques which we discuss in some detail.

In Sec. 3 it emerges that higher order schemes allow a significant reduction of the degrees of freedom without sacrificing accuracy. For some applications it may be natural to consider the ultimate limit, leading to global or spectral methods as discussed in Sec. 5. As tempting as this approach is, the need for geometric flexibility again enters as a major concern. We discuss in some detail the elements of spectral multi-domain methods, which combine the accuracy of global methods with the geometric flexibility of a multi-element formulation.

The need to decompose the computational domain into multiple elements to maintain accuracy and geometric flexibility is not unique to computational electromagnetics and it is only natural that much work has focused on transferring successes from other branches of science into the time-domain solution of Maxwell's equations. An example of this is discussed in Sec. 6 where recent efforts on the development of high-order finite volume methods, recovered by considering Maxwell's equations as a system of conservation laws, is outlined. A parallel and more extensive effort focuses on the development of finite element methods for solving Maxwell's equations in the time-domain. This, as discussed in Sec. 7, is more involved and requires attention to a number of issues, e.g., proper form of the equations, proper variational statement, and element types. We shall discuss some possibilities and recent developments before turning the attention to discontinuous element schemes which we discuss in some detail due to their attractive properties for problems such as Maxwell's equations. As we shall see, the finite element formulations are in general the mathematically most complex but also result in formulations which appear most promising at this point in time, assuming – naively – that the associated grid-generation is a minor issue. We conclude, in Sec. 8, with a brief discussion of issues related to high-order time stepping and discrete stability, before offering a few concluding remarks in Sec. 9.

2. MAXWELL'S EQUATIONS IN THE TIME-DOMAIN

We concern ourselves with the direct solution of Maxwell's equations on differential form

$$\frac{\partial \tilde{\boldsymbol{D}}}{\partial \tilde{t}} = \tilde{\nabla} \times \tilde{\boldsymbol{H}} + \tilde{\boldsymbol{J}} \quad , \quad \frac{\partial \tilde{\boldsymbol{B}}}{\partial \tilde{t}} = -\tilde{\nabla} \times \tilde{\boldsymbol{E}} \quad , \tag{1}$$

$$\tilde{\nabla} \cdot \tilde{\boldsymbol{D}} = \tilde{\rho} \ , \ \ \tilde{\nabla} \cdot \tilde{\boldsymbol{B}} = 0 \ , \tag{2}$$

in the three-dimensional domain, Ω, with the charge distribution, $\tilde{\rho}(\tilde{\boldsymbol{x}}, \tilde{t})$. The electric field, $\tilde{\boldsymbol{E}}(\tilde{\boldsymbol{x}}, \tilde{t})$, and the electric flux density, $\tilde{\boldsymbol{D}}(\tilde{\boldsymbol{x}}, \tilde{t})$, as well as the magnetic field, $\tilde{\boldsymbol{H}}(\tilde{\boldsymbol{x}}, \tilde{t})$, and the magnetic flux density, $\tilde{\boldsymbol{B}}(\tilde{\boldsymbol{x}}, \tilde{t})$, are related through the constitutive relations

$$\tilde{\boldsymbol{D}} = \tilde{\boldsymbol{\varepsilon}} \tilde{\boldsymbol{E}} \ , \ \ \tilde{\boldsymbol{B}} = \tilde{\boldsymbol{\mu}} \tilde{\boldsymbol{H}} \ .$$

The permittivity tensor, $\tilde{\boldsymbol{\varepsilon}}$, and the permeability tensor, $\tilde{\boldsymbol{\mu}}$, are in general anisotropic and may depend on space and time as well as the strength of the fields themselves. The current, $\tilde{\boldsymbol{J}}$, is typically assumed to be related to the electric field, $\tilde{\boldsymbol{E}}$, through Ohms law, $\tilde{\boldsymbol{J}} = \tilde{\sigma} \tilde{\boldsymbol{E}}$, where $\tilde{\sigma}$ measures the finite conductivity, although more complex relations are possible.

In the subsequent discussion, we shall generally assume that the materials can be assumed isotropic, linear, and time-invariant. In that case the constitutive relations take the form

$$\tilde{\boldsymbol{D}} = \tilde{\varepsilon}_0 \varepsilon_r \tilde{\boldsymbol{E}} \ , \ \ \tilde{\boldsymbol{B}} = \tilde{\mu}_0 \mu_r \tilde{\boldsymbol{H}} \ .$$

Here $\tilde{\varepsilon}_0 = 8.854 \times 10^{-12}$ F/m and $\tilde{\mu}_0 = 4\pi \times 10^{-7}$ H/m represent the vacuum permittivity and permeability, respectively, and $\varepsilon_r(\boldsymbol{x})$ and $\mu_r(\boldsymbol{x})$ refers to the relative permittivity and permeability, respectively, of the materials.

It is worth while pointing out, however, that most of the methods discussed in the following can be extended to include much more complex and even nonlinear materials with limited additional effort required.

Taking the divergence of Eq.(1) and applying Eq.(2) in combination with Gauss' law for charge conservation shows that if the initial conditions satisfy Eq.(2), and the fields are evolved according to Maxwell's equations, Eq.(1), the solution will satisfy Eq.(2) at all times. Hence, one generally views Eq.(2) as a consistency relation on the initial conditions and limit the solution to the time-dependent part of Maxwell's equations, Eq.(1), although the validity of doing so remains somewhat controversial [65, 72]

To simplify matters further, we consider the non-dimensionalized equations by introducing the normalized quantities

$$\boldsymbol{x} = \frac{\tilde{\boldsymbol{x}}}{\tilde{L}} \ , \ \ t = \frac{\tilde{t}}{\tilde{L}/\tilde{c}_0} \ ,$$

where $\tilde{L}$ is a reference length, and $\tilde{c}_0 = (\tilde{\varepsilon}_0 \tilde{\mu}_0)^{-1/2}$ represents the dimensional vacuum speed of light. The fields themselves are normalized as

$$\boldsymbol{E} = \frac{\tilde{Z}_0^{-1} \tilde{\boldsymbol{E}}}{\tilde{H}_0} \ , \ \ \boldsymbol{H} = \frac{\tilde{\boldsymbol{H}}}{\tilde{H}_0} \ , \ \ \boldsymbol{J} = \frac{\tilde{\boldsymbol{J}} \tilde{L}}{\tilde{H}_0} \ ,$$

where $\tilde{Z}_0 = \sqrt{\tilde{\mu}_0/\tilde{\varepsilon}_0}$ refers to the dimensional free space intrinsic impedance, and $\tilde{H}_0$ is a dimensional reference magnetic field strength.

With this normalization Eq.(1) takes the form

$$\varepsilon_r \frac{\partial \boldsymbol{E}}{\partial t} = \nabla \times \boldsymbol{H} + \boldsymbol{J} \quad , \quad \mu_r \frac{\partial \boldsymbol{H}}{\partial t} = -\nabla \times \boldsymbol{E} \ , \tag{3}$$

which is the form of the equations we shall consider in what remains. The components of the fields are subsequently referred to as $\boldsymbol{E} = (E^x, E^y, E^z)^T$ and likewise for $\boldsymbol{H}$ and $\boldsymbol{J}$.

To solve Maxwell's equations in the vicinity of boundaries, penetrable or not, we shall need boundary conditions relating the field components on either side of the boundary. Assuming that a normal unit vector, $\hat{\boldsymbol{n}}$, to the boundary is given, the boundary conditions on the electric field components take the form

$$\hat{\boldsymbol{n}} \times (\boldsymbol{E}_1 - \boldsymbol{E}_2) = 0 \ , \ \ \hat{\boldsymbol{n}} \cdot (\boldsymbol{D}_1 - \boldsymbol{D}_2) = \rho_s \ ,$$

where $\boldsymbol{E}_i$ and $\boldsymbol{D}_i$, $i = (1, 2)$, represent the fields on either side of the interface and ρ_s represents a surface charge. Equivalently, the conditions on the magnetic fields are given as

$$\hat{\boldsymbol{n}} \times (\boldsymbol{H}_1 - \boldsymbol{H}_2) = \boldsymbol{J}_s \ , \ \ \hat{\boldsymbol{n}} \cdot (\boldsymbol{B}_1 - \boldsymbol{B}_2) = 0 \ ,$$

where $\boldsymbol{J}_s$ represents a surface current density.

In the general case of materials with finite conductivity, no surface charges and currents can exist, and the relevant conditions become

$$\hat{\boldsymbol{n}} \times (\boldsymbol{E}_1 - \boldsymbol{E}_2) = 0 \ , \ \ \hat{\boldsymbol{n}} \times (\boldsymbol{H}_1 - \boldsymbol{H}_2) = 0 \ , \tag{4}$$

expressing continuity of the tangential field components. The normal components of the flux densities must likewise satisfy

$$\hat{\boldsymbol{n}} \cdot (\boldsymbol{D}_1 - \boldsymbol{D}_2) = 0 \ , \ \ \hat{\boldsymbol{n}} \cdot (\boldsymbol{B}_1 - \boldsymbol{B}_2) = 0 \ , \tag{5}$$

i.e., they are continuous, while the normal components of the fields themselves are discontinuous.

For the important special case of a perfect conductor, the conditions take a special form as the perfect conductor supports surface charges and currents while the fields are unable to penetrate into the body, i.e.,

$$\hat{\boldsymbol{n}} \times \boldsymbol{E} = 0 \ , \ \ \hat{\boldsymbol{n}} \cdot \boldsymbol{B} = 0 \ . \tag{6}$$

2.1. The Scattered Field Formulation

For scattering and penetration problems involving linear materials it is often advantageous to exploit the linearity of Maxwell's equations and solve for the scattered field, $(\boldsymbol{E}^{\mathrm{s}}, \boldsymbol{H}^s)$, rather than for the total field, $(\boldsymbol{E}, \boldsymbol{H})$. These are trivially related as

$$\boldsymbol{E} = \boldsymbol{E}^i + \boldsymbol{E}^s \ , \ \boldsymbol{H} = \boldsymbol{H}^i + \boldsymbol{H}^s \ ,$$

where $(\boldsymbol{E}^i, \boldsymbol{H}^i)$ represents the incident field, illuminating the scattering object.

A particularly useful illumination is the vacuum plane wave of the form

$$\boldsymbol{E}^i = \boldsymbol{A} \exp\left[i 2\pi \frac{L}{\lambda} \left(\hat{\boldsymbol{k}} \cdot \boldsymbol{x} - \nu t \right) \right] \ , \ \boldsymbol{H}^i = \hat{\boldsymbol{k}} \times \boldsymbol{E}^i \ .$$

Here $\hat{\boldsymbol{k}} = (\hat{k}_x, \hat{k}_y, \hat{k}_z)^T$ is normalized wave vector and ν the normalized frequency. One can think of L/λ as a normalized inverse wavelength of the illuminating wave. For monochromatic plane wave illumination, it is customary to take $L = \lambda$ to simplify matters.

Assuming that $(\boldsymbol{E}^i, \boldsymbol{H}^i)$ represents a particular solution, e.g., the plane wave solution give above, to Maxwell's equations, one recovers the scattered field formulation

$$\varepsilon_r \frac{\partial \boldsymbol{E}^s}{\partial t} = \nabla \times \boldsymbol{H}^s + \sigma \boldsymbol{E}^s - \left(\varepsilon_r - \varepsilon_r^i \right) \frac{\partial \boldsymbol{E}^i}{\partial t} + (\sigma - \sigma^i) \boldsymbol{E}^i \ , \tag{7}$$

$$\mu_r \frac{\partial \boldsymbol{H}^s}{\partial t} = -\nabla \times \boldsymbol{E}^s - \left(\mu_r - \mu_r^i \right) \frac{\partial \boldsymbol{H}^i}{\partial t} \ , \tag{8}$$

where $\varepsilon_r^i(\boldsymbol{x})$, $\mu_r^i(\boldsymbol{x})$, and $\sigma^i(\boldsymbol{x})$ represents the relative permittivity, permeability and conductivity of the media in which the incident field is a solution to Maxwell's equations, e.g., in the above case of a plane wave vacuum field illuminating the object we have $\varepsilon_r^i = \mu_r^i = 1$, and $\sigma^i = 0$. To simplify matters we have assumed Ohms law, $\boldsymbol{J} = \sigma \boldsymbol{E}$.

In this formulation, the boundary conditions along a dielectric interface are

$$\hat{\boldsymbol{n}} \times (\boldsymbol{E}_1^s - \boldsymbol{E}_2^s) = 0 \ , \ \hat{\boldsymbol{n}} \times (\boldsymbol{H}_1^s - \boldsymbol{H}_2^s) = 0 \ , \tag{9}$$

for the tangential components, while the conditions on the scattered field components becomes

$$\hat{\boldsymbol{n}} \times \boldsymbol{E}^s = -\hat{\boldsymbol{n}} \times \boldsymbol{E}^i \ , \ \hat{\boldsymbol{n}} \cdot \boldsymbol{B}^s = -\mu_r \hat{\boldsymbol{n}} \cdot \boldsymbol{H}^i \ , \tag{10}$$

in the case of a perfectly conducting boundary. The general conditions on normal components can likewise be derived directly from Eq.(5).

2.2. Maxwell's Equations in One and Two-Dimensions

For completeness, let us also state Maxwell's equations in the one- and two-dimensional cases. In the former case we simply have

$$\varepsilon_r \frac{\partial E^z}{\partial t} = \frac{\partial H^z}{\partial x} + J^z \quad , \quad \mu_r \frac{\partial H^z}{\partial t} = \frac{\partial E^z}{\partial x} \quad . \tag{11}$$

Both field components are tangential to a material interface and, thus, always continuous – but not smoother than that. At a metallic boundary, E^z vanishes. This set of equations is well suited for testing new schemes as it captures essential features of Maxwell's equations, e.g., two-way wave propagation and loss of smoothness across material interfaces.

To model effects of polarization, reflection/refraction at interfaces, diffraction etc we need to consider two dimensional problems. In this case Maxwell's equations separate into two independent cases – polarizations – with the transverse electric (TE) form being

$$\begin{aligned} \varepsilon_r \frac{\partial E^x}{\partial t} &= \frac{\partial H^z}{\partial y} + J^x \quad , \\ \varepsilon_r \frac{\partial E^y}{\partial t} &= -\frac{\partial H^z}{\partial x} + J^y \quad , \\ \mu_r \frac{\partial H^z}{\partial t} &= \frac{\partial E^x}{\partial y} - \frac{\partial E^y}{\partial x} \quad , \end{aligned} \tag{12}$$

by assuming that $E^z = 0$ and $\frac{\partial}{\partial z} = 0$. The other polarization, known as the transverse magnetic (TM) form, is given as

$$\begin{aligned} \mu_r \frac{\partial H^x}{\partial t} &= -\frac{\partial E^z}{\partial y} \quad , \\ \mu_r \frac{\partial H^y}{\partial t} &= \frac{\partial H^z}{\partial x} \quad , \\ \varepsilon_r \frac{\partial E^z}{\partial t} &= \frac{\partial H^y}{\partial x} - \frac{\partial H^x}{\partial y} + J^z \quad , \end{aligned} \tag{13}$$

by taking $H^z = 0$.

Boundary conditions and scattered field forms can be derived as for the general case discussed previously.

3. THE CASE FOR HIGH-ORDER METHODS IN CEM

To come to an appreciation of the need for high-order methods in time-domain electromagnetics, let us briefly recall the question of phase-errors associated with finite-difference methods, as first presented in the pioneering work of Kreiss and Oliger [80].

Consider, as the fundamental component of Maxwell's equations, the scalar wave equation

$$\frac{\partial u}{\partial t} = -c \frac{\partial u}{\partial x} \quad , \quad u(x,0) = e^{ikx} \quad ,$$

in the domain $x \in [0, 2\pi]$ and subject to periodic boundary conditions. Here $k = 2\pi/\lambda$ is the wavenumber. To begin with, we consider only the effect of the spatial

approximation and restrict the discussion to finite difference methods. One should keep in mind, however, that the conclusions reaches remain qualitatively true also for the other high-order accurate schemes discussed subsequently.

We introduce an equidistant grid

$$x_j = \frac{2\pi j}{N} = jh \ , \ \ j \in [0, N-1] \ ,$$

such that $u(x_j, t) = u_j$. Using a $2m$'th order explicit central difference approximation to the spatial derivative of $u(x,t)$ yields the semi-discrete scheme

$$\left.\frac{du}{dt}\right|_{x_j} = -c \sum_{n=1}^{m} \left(\frac{-2(-1)^n (m!)^2}{(m-n)!(m+n)!} \right) \frac{1}{2n} \mathrm{D}_n u_j \ ,$$

where

$$\mathrm{D}_n = \frac{\mathrm{E}_n - \mathrm{E}_{-n}}{h} \ , \ \ \mathrm{E}_n u_j = u_{j+n} \ , \tag{14}$$

represents the central difference and shift operator, respectively.

The exact solution to this semi-discrete equation is

$$u(x,t) = e^{ik(x - c_m(k)t)} \ .$$

Here $c_m(k)$ is termed the numerical wave speed. Clearly we wish that $c \simeq c_m(k)$ over as large a range of the wavenumber, k, as possible. A measure of this, the phase error, is defined as

$$e_m(k) = |k(c - c_m(k))t| \ .$$

The analysis of the phase error allows us to answer questions about the proper choice of schemes for a specified phase error and the overall efficiency of high-order methods.

To continue, let us introduce non-dimensional measures of the actual scheme. In particular, we introduce

$$p = \frac{\lambda}{h} = \frac{2\pi}{kh} \ , \ \ \nu = \frac{ct}{\lambda} \ ,$$

which are nothing else than the number of points per wavelength, p, and the number of wave-periods, ν, we wish to advance the wave. The phase-error thus becomes

$$e_m(p, \nu) \simeq \frac{\pi \nu}{\alpha_m} \left(\frac{2\pi}{p} \right)^{2m} \ ,$$

where α_m is a constant specific to the truncation error of the different schemes, e.g. $\alpha_1 = 3$, $\alpha_2 = 15$, $\alpha_3 = 70$ [80] etc. If we term the maximal acceptable phase-error, ε_p, we recover the lower bounds

$$p_m(\nu, \varepsilon_p) \geq 2\pi \sqrt[2m]{\frac{\nu\pi}{\alpha_m \varepsilon_p}} \propto \sqrt[2m]{\frac{\nu}{\varepsilon_p}} \ , \tag{15}$$

on the number of points per wavelengths, $p_m(\nu, \varepsilon_p)$, required to ensure a specified error, ε_p, after ν periods of propagation. We note that the required number of points per wavelength depend on the acceptable accuracy, ε_p, but also on the number of periods, ν, needed to complete the computation, i.e. the effect of the phase-error accumulates over time.

Assume now that we wish to propagate a wave in a d-dimensional box with side lengths λ. Clearly, considering general problems of size $L\lambda$ simply scales all results with L^d.

The memory needed to store the fields is proportional to

$$\text{Memory} \propto (p_m)^d \propto \left(\frac{\nu}{\varepsilon_p}\right)^{\frac{d}{2m}} .$$

Furthermore, the work needed to advance the solution to the final time, t, scales as

$$\text{Work} \propto (2mp_m)^d \frac{t}{\Delta t} \propto (2m)^d \nu \left(\frac{\nu}{\varepsilon_p}\right)^{\frac{d+1}{2m}} .$$

The strong dependence on $2m$, i.e., the order of the scheme, suggests that using high-order schemes ($m > 1$) is advantageous when measured in memory usage and/or required computational work in the following situations

- $\varepsilon_p \ll 1$, i.e., when high accuracy is required.
- $\nu \gg 1$, i.e., when long time integration is needed.
- $d > 1$, i.e., for multi-dimensional problems.
- $p_m < 10$, i.e., efficient discretizations of large problems.

These are clearly situations of relevance to the modeling of electromagnetic phenomena. While this analysis does not include effects of grid-anisotropy on the wave-propagation, this is only to benefit of the low-order schemes which will suffer most from such phenomena. Furthermore, the popular use of staggered grids will not improve the efficiency of the low-order methods qualitatively [127].

Thus, the use of high-order accurate methods promises to enable the accurate and efficient modeling of transient electrically large problems over long times. It is the purpose of what remains to discuss a number of recently developed computational methods that aims at fulfilling these promises.

4. HIGH-ORDER FINITE DIFFERENCE SCHEMES

The most widely used computational technique for solving Maxwell's equations in the time-domain, the finite-difference time-domain (FDTD) method, can be traced to a scheme introduced by Yee [132]. It utilizes the special structure of Maxwell's equations and introduces a spatially staggered equidistant grid in which the problem of interest is embedded.

Let us introduce $u_i = u(x_i)$ as a grid function defined on an equidistant grid, x_i, with grid size, h. Using the notation of Eq.(14), the familiar 2nd order central finite difference scheme is

$$\frac{du_i}{dx} = \tfrac{1}{2}\mathrm{D}_1 u_i \ .$$

To recover a semi-discrete approximation to Eq.(11) we define a set of staggered grids, x_i and $x_{i+1/2}$, shifted space by $h/2$, on which E and H are collocated, respectively. This yields

$$\varepsilon(x_i)\frac{dE_i^z}{dt} = \mathrm{D}_{1/2}H_i^z \quad ,$$

$$\mu(x_{i+1/2})\frac{dH_{i+1/2}^z}{dt} = \mathrm{D}_{1/2}E_{i+1/2}^z \quad .$$

We assume, for simplicity, no currents, i.e., $J^z = 0$. Approximating the temporal integration by a staggered-in-time leap-frog scheme yields

$$\varepsilon(x_i)\frac{E_i^{n+1} - E_i^n}{\Delta t} = \mathrm{D}_{1/2}H_i^{n+1/2} \quad ,$$

$$\mu(x_{i+1/2})\frac{H_{i+1/2}^{n+1/2} - H_{i+1/2}^{n-1/2}}{\Delta t} = \mathrm{D}_{1/2}E_{i+1/2}^n \quad ,$$

which is indeed the classic Yee scheme, proposed in [132]. Here $E_i^n = E^z(x_i, n\Delta t)$ and similarly for H^z. In regions with smoothly varying materials, this scheme is 2nd order accurate in space and time.

The success of the Yee scheme, combined with the realization that 2nd order accuracy may well be insufficient for many applications, has spawned much recent work in the development of higher order accurate schemes of a similar nature. To highlight the problems associated with such extensions, let us consider a simple example.

Consider the one-dimensional problem,

$$\varepsilon_r(x)\frac{\partial E^z}{\partial t} = \frac{\partial H^z}{\partial x} \quad , \quad \frac{\partial H^z}{\partial t} = \frac{\partial E^z}{\partial x} \quad ,$$

defined in the domain $x \in [-L, L]$ and with a material interface positioned at $x = a, |a| < L$ and metallic walls at $|x| = L$, i.e., $E_z(\pm L, t) = 0$. The permittivity is assumed to be piecewise constant as

$$\varepsilon_r(x) = \begin{cases} \varepsilon_r^{(1)} & -L \le x \le a \\ \varepsilon_r^{(2)} & a < x < L \end{cases} \quad .$$

One easily derives the exact solution of this problem, essentially consisting of a set of standing waves, as illustrated in Fig. 1. The exact solution is given in [24].

In Fig. 1 we show an example of the solution and the results obtained using a straightforward 4th order extension of the Yee scheme, discussed in Sec. 4.1. For the simple homogeneous problem we see the expected 4th order convergence. A 4th order explicit Runge-Kutta scheme is used to advance in time, and the global discrete L^2-norm measures the error, i.e.,

$$\|u\|_h = \left(h \sum_{i=0}^{N} u_i^2 \right)^{1/2} \quad , \quad h = \frac{2L}{N} \quad ,$$

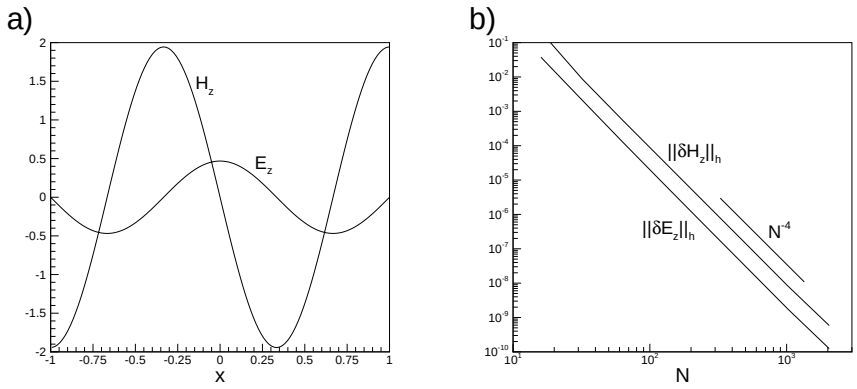

FIG. 1. Metallic cavity problem, $L = 1$, $\varepsilon_r = 1$ and the final time for computation is $T = 2\pi$. In a) we show the solution at $T = 2\pi$ and in b) we confirm the expected 4th order global convergence as a function of number of points, N.

and δu signifies the difference between the computed and the exact solution.

While such straightforward extensions of the Yee scheme performs well for homogeneous problems with grid-conforming geometries, these schemes also inherit the problems associated with the Yee-scheme, i.e., the need to staircase general geometries and the inability to correctly enforce physical jump-conditions, Eqs.(4)-(5), at material interfaces.

While a consequence of such staircasing is accuracy reduction , i.e., one is solving a problem that is $\mathcal{O}(h)$ different, is well established in the literature (see e.g. [24]), it appears less appreciated that the physical interface conditions at a material interface are equally important. To emphasize this point, we show in Fig. 2 results for the cavity problem discussed above, assuming, however, that for $x \in [0, L]$ the cavity is filled with an $\varepsilon_r^{(2)} = 2.25$ material. While the solution remains continuous across the material interface, it does not remain smooth, i.e., using a difference scheme across the interface is poised to have a reduced accuracy as is also confirmed in Fig. 2. The popular use of averaging of the material coefficients [116, 19] restores $\mathcal{O}(h^2)$ accuracy only.

One should keep in mind that the situation may well be worse for multi-dimensional problems where the averaging technique is much less effective due to the likely existence of discontinuous fields. Indeed, one can construct simple tests where even the Yee scheme fails to converge due to this [24].

Thus, the formulation of high-order finite-difference methods entails not only the derivation of the high-order accurate finite-difference stencils but also techniques to treat the embedded geometries to the order of the scheme. The latter is considerably more complex than the former as some of the approaches discussed in the following illustrate.

4.1. Extensions of the Yee Scheme

It is a simple matter to derive a direct higher order accurate finite difference stencil on a staggered grid, i.e., we have the explicit 4th order scheme

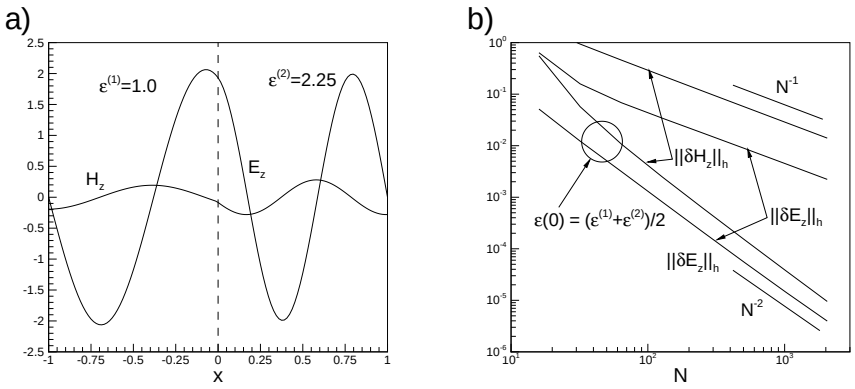

FIG. 2. Metallic cavity problem, $L = 1$, $\varepsilon_r^{(1)} = 1.0, \varepsilon_r^{(2)} = 2.25$, and the final time for computation is $T = 2\pi$. In a) we show the solution at $T = 2\pi$ and in b) we illustrate the global convergence as a function of number of points, N, using a straightforward 4th order scheme as well as one making use of an averaged material parameter.

$$\begin{aligned} \varepsilon(x_i)\frac{dE_i^z}{dt} &= \tfrac{1}{24}\left(27\mathrm{D}_{1/2} - \mathrm{D}_{3/2}\right) H_i^z \quad , \\ \mu(x_{i+1/2})\frac{dH_{i+1/2}^z}{dt} &= \tfrac{1}{24}\left(27\mathrm{D}_{1/2} - \mathrm{D}_{3/2}\right) E_{i+1/2}^z \quad . \end{aligned} \tag{16}$$

This appears to have been considered first in the context of electromagnetics in [29] as a direct extension of the Yee scheme, i.e., using a second order accurate scheme in time. Subsequent works using this approach include [101, 100, 117]. Results, combining this with the Yee scheme in subgridded areas, are obtained in [36, 37].

Close to metallic boundaries one can use 3rd order closures of the form

$$\varepsilon(x_i)\frac{dE_i^z}{dt} = \frac{-23H_{i-1/2}^z + 21H_{i+1/2}^z + 3H_{i+3/2}^z - H_{i+5/2}^z}{24h} \quad , \tag{17}$$

which suffices to ensure global 4th order accuracy [43]. This is the scheme used on the examples shown in Figs. 1 and 2. A stable 4th order closure is proposed in [134].

While one may continue such developments and define stencils of arbitrary order, such methods has little practical value as the corresponding one-sided closures tend to be unstable [114, 44]. We shall therefore restrict the attention to the 4th order scheme above, as has been done in most of the current literature.

Attempting to overcome the problems exposed above the solution escapes the obvious, e.g., using a high order approximation to the material properties [117, 135] may improve matters quantitatively but not make a qualitative difference, i.e., the convergence rate typically remains 2nd order. Furthermore, the extension of such techniques to multi-dimensional problems, where higher order geometric information, e.g., curvature, would need to enter the model to maintain design accuracy, remains elusive.

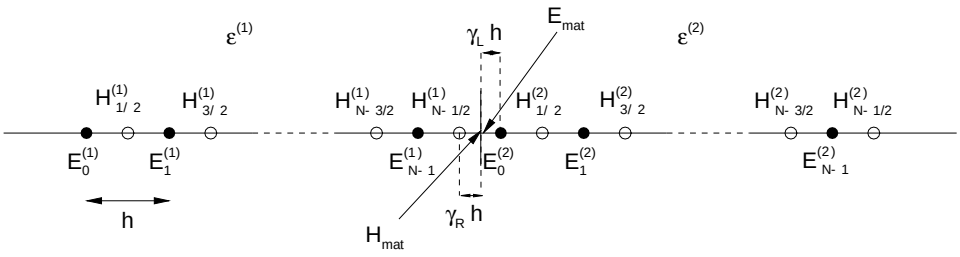

FIG. 3. Definition of grid, numbering and various parameters for solving the one-dimensional Maxwell's equations in a PEC cavity filled with two materials.

Initiated in [24] in the context of Maxwell's equations, steps in a different direction has recently been taken. The central idea is to use the staggered grid scheme, Eqs.(16)-(17), in homogeneous regions away from boundaries and then locally modify the scheme close to boundaries and interfaces. This latter part must be done in a geometry conforming way to overcome the staircasing problem and must include the physically correct jump conditions. As shown in [24] such schemes, termed embedding schemes, allow one to fully restore 2nd order accuracy in a modified Yee scheme, thus overcoming problems of staircasing and the effect internal boundaries in a unified way. As the scheme is modified locally only, it maintains the simplicity and computational efficiency of the original formulation as most of the additional work, i.e., computing the local stencils, is done in a preprocessing stage.

The extension of these ideas to 4th order embedding methods is far from trivial and questions remain unanswered. To illustrate the potential of such methods, however, let us return to the cavity problem above but allow the material interface to be positioned anywhere inside the cavity, i.e., we do not require geometric conformity.

We shall use Fig. 3 to highlight the elements of the scheme. Everywhere away from the internal material boundary we use the 4th order staggered grid method given in Eqs.(16)-(17). Also, grid-points not directly adjacent to the interface, e.g., $E^{(1)}_{N-1}$ and $H^{(2)}_{1/2}$ is updated using the one-sided 3rd order scheme, Eq.(17), reaching into the homogeneous region. The critical question is naturally to update the points directly next to the interface, i.e., $H^{(1)}_{N-1/2}$ and $E^{(2)}_0$. The idea put forward in [24] is to form extrapolated valued, $H_{\rm mat}$ and $E_{\rm mat}$, from the left and right, respectively, and use these in combination with the physical jump-conditions to complete the scheme.

Using the notation of Fig. 3, we define the extrapolated fields as

$$\begin{aligned} H_{\rm mat} = \quad & \frac{(7-2\gamma_L)(5-2\gamma_L)(3-2\gamma_L)}{48} H^{(1)}_{N-1/2} - \frac{(7-2\gamma_L)(5-2\gamma_L)(1-2\gamma_L)}{16} H^{(1)}_{N-3/2} \\ & + \frac{(7-2\gamma_L)(3-2\gamma_L)(1-2\gamma_L)}{16} H^{(1)}_{N-5/2} - \frac{(5-2\gamma_L)(3-2\gamma_L)(1-2\gamma_L)}{48} H^{(1)}_{N-7/2} \end{aligned}$$

and

$$E_{\text{mat}} = \frac{(7-2\gamma_R)(5-2\gamma_R)(3-2\gamma_R)}{48}E_0^{(2)} - \frac{(7-2\gamma_R)(5-2\gamma_R)(1-2\gamma_R)}{16}E_1^{(2)} + \frac{(7-2\gamma_R)(3-2\gamma_R)(1-2\gamma_R)}{16}E_2^{(2)} - \frac{(5-2\gamma_R)(3-2\gamma_R)(1-2\gamma_R)}{48}E_3^{(2)}$$

Note that due to the geometry of the problem, $\gamma_L + \gamma_R = \frac{1}{2}$. The schemes to update $H_{N-1/2}^{(1)}$ and $E_0^{(2)}$ are then given as

$$\frac{dH_{N-1/2}^{(1)}}{dt} = \frac{46}{h(1+2\gamma_L)(3+2\gamma_L)(5+2\gamma_L)}E_{\text{mat}} - \frac{15-16\gamma_L}{4h(1+2\gamma_L)}E_{N-1}^{(1)} + \frac{5-12\gamma_L}{2h(3+2\gamma_L)}E_{N-2}^{(1)} - \frac{3-8\gamma_L}{4h(5+2\gamma_L)}E_{N-3}^{(1)} \ ,$$

and

$$\varepsilon^{(2)}\frac{dE_0^{(2)}}{dt} = -\frac{46}{h(1+2\gamma_R)(3+2\gamma_R)(5+2\gamma_R)}H_{\text{mat}} + \frac{15-16\gamma_R}{4h(1+2\gamma_R)}H_{1/2}^{(2)} - \frac{5-12\gamma_R}{2h(3+2\gamma_R)}H_{3/2}^{(2)} + \frac{3-8\gamma_R}{4h(5+2\gamma_R)}H_{5/2}^{(2)} \ .$$

It is worth emphasizing that the stencils do not collapse even if the interface is positioned very close to or at a grid point. This is a consequence of the staggered grid which is essential to ensure this and yield a scheme with a uniformly bounded time-step restriction.

As an illustration of the performance of the scheme we show in Fig. 4 results obtained for the problem discussed in relation to Fig. 2, although allowing the interface to be positioned away from a grid point also. In such a situation the unmodified scheme would yield only $\mathcal{O}(h)$ convergence due to staircasing. However, as shown in 4, the embedded scheme recovers full accuracy regardless of the position of the material interface.

Albeit less general, similar ideas exploiting locally modified explicit schemes have also been developed in [134]. There the position of the interface is restricted to coincide with the grid points but the physical jump-conditions are enforced as above. A slight generalization along similar lines is found in [126] where such ideas are combined with smooth curvilinear mappings. In [102] it is discussed how the embedding can be utilized as a separator between different grids rather than different materials, thus allowing for subgridding.

While the embedding schemes are appealing and appears to offer a good balance between computational complexity and obtainable accuracy, much development remains to be done to make these methods a viable alternative. In particular, the stable and accurate treatment of curved interfaces and metallic boundaries remains a challenge.

In [121, 122] a related, yet slightly different approach is taken. Motivated by [118], the authors apply dispersion-relation-preserving (DRP) 4th order explicit schemes to solve Maxwell's equations in two [121] and three [122] spatial dimensions. Such schemes are derived by extending the stencil beyond the minimum 5 points. The

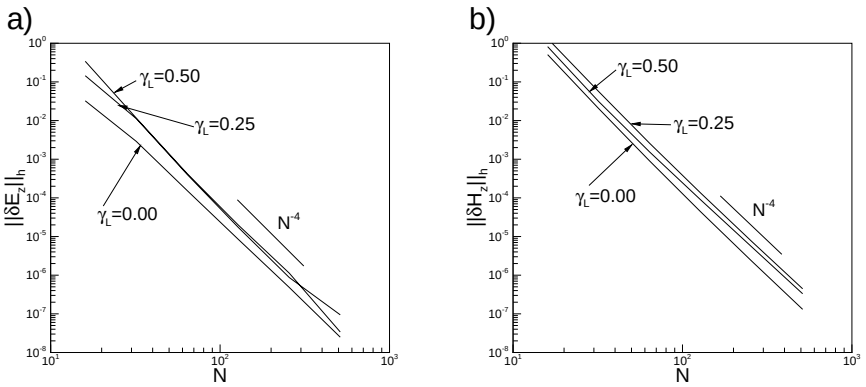

FIG. 4. Same problem as in Fig. 2, however solved using the 4th order embedding scheme. In a) we illustrate the global convergence of E^z while b) illustrates the same for H^z.

additional degrees of freedom for defining the stencil is used to optimize its wave-propagation characteristics, e.g., by minimizing the phase-error. While such an approach is highly accurate wave-propagation, the wide stencil makes it difficult to terminate the stencil and, thus, deal with complex geometries.

4.2. Compact Schemes and SBP Schemes

The problems with stability and accuracy of the straightforward 4th order extension of the Yee scheme, Eq.(16), discussed above has lead to a number of alternative developments. These have mostly focused on implicit computations of the derivatives, i.e.,

$$\mathrm{P}\frac{d}{dx}\boldsymbol{u} = \mathrm{Q}\boldsymbol{u} \quad . \tag{18}$$

Here $\boldsymbol{u}$ represents the grid-vector and the two matrices, P and Q, are constructed to ensure accuracy and/or stability of the approximation.

A classical example of such methods are the compact schemes, see e.g. [84] for an introduction. These were introduced in the context of Maxwell's equations in [117, 106, 135].

Let us for illustration continue the use of a staggered grid as above. Then, the classical 4th order compact scheme for computing derivatives is [117]

$$\left(\frac{1}{2}\Delta x\mathrm{D}_1 + 11\right)\frac{du_i}{dx} = 12\mathrm{D}_{1/2}u_i \quad ,$$

i.e., it is an implicit scheme, involving the solution of a tridiagonal matrix. Its main appeal lies in a very compact stencil, using only nearest neighbor values, and better accuracy than explicit schemes discussed above. Furthermore, away from boundaries and interfaces, the scheme conserves divergence due to the staggered grid.

Close to boundaries special stencils are needed as for the explicit scheme. In [135, 117] a fully implicit closures is proposed on the form

$$26\frac{du_{1/2}}{dx} - 5\frac{du_{3/2}}{dx} + 4\frac{du_{5/2}}{dx} - \frac{du_{7/2}}{dx} = 24\mathrm{D}_{1/2}u_{1/2} \quad .$$

Combining these expressions yields

$$\mathrm{P} = \frac{1}{24}\begin{bmatrix} 26 & -5 & 4 & -1 & . & . & . & 0 \\ 1 & 22 & 1 & 0 & . & . & . & 0 \\ 0 & 1 & 22 & 1 & 0 & . & . & 0 \\ . & . & . & . & . & . & . & . \\ . & . & . & . & . & . & . & . \\ 0 & . & . & . & 1 & 22 & 1 & 0 \\ 0 & . & . & . & 0 & 1 & 22 & 1 \\ 0 & . & . & . & -1 & 4 & -5 & 26 \end{bmatrix} \quad ,$$

and

$$\mathrm{Q} = \frac{1}{\Delta x}\begin{bmatrix} -1 & 1 & 0 & 0 & . & . & . & 0 \\ 0 & -1 & 1 & 0 & . & . & . & 0 \\ 0 & 0 & -1 & 1 & 0 & . & . & 0 \\ . & . & . & . & . & . & . & . \\ . & . & . & . & . & . & . & . \\ 0 & . & . & 0 & -1 & 1 & 0 & 0 \\ 0 & . & . & . & 0 & -1 & 1 & 0 \\ 0 & . & . & . & 0 & 0 & -1 & 1 \end{bmatrix} \quad ,$$

we recover the 4th order semi-discrete compact scheme for the one-dimensional Maxwell's equations as

$$\varepsilon_r \frac{d\boldsymbol{E}_h^z}{dt} = \mathrm{P}^{-1}\mathrm{Q}\boldsymbol{H}_h^z \quad , \quad \boldsymbol{\mu}_r \frac{d\boldsymbol{H}_h^z}{dt} = \mathrm{P}^{-1}\mathrm{Q}\boldsymbol{E}_h^z \quad .$$

We have introduced the vectors of grid-functions

$$\boldsymbol{E}_h^z = \left[E_0^z(t), E_1^z(t), .., E_{N-1}^z(t), E_N^z(t)\right]^T \quad ,$$

$$\boldsymbol{H}_h^z = \left[H_{1/2}^z(t), H_{3/2}^z(t), .., H_{N-3/2}^z(t), H_{N-1/2}^z(t)\right]^T \quad ,$$

and similarly for the vectors of materials

$$\boldsymbol{\varepsilon}_r = \left[\varepsilon_r(x_0), \varepsilon_r(x_1), .., \varepsilon_r(x_{N-1}), \varepsilon_r(x_N)\right]^T \quad ,$$

$$\boldsymbol{\mu}_r = \left[\mu_r(x_{1/2}), \mu_r(x_{3/2}), .., \mu_r(x_{N-3/2}), \mu_r(x_{N-1/2})\right]^T \quad .$$

Since P is banded its inversion is cheap. Results in [117, 135] confirm the expected accuracy and stability of the scheme for the one-dimensional Maxwell equations and the two-dimensional TM-form, Eq.(13), assuming simple grid conforming boundaries and homogeneous materials. Dispersion-relation-preserving compact schemes are discussed in [84].

Although the compact scheme achieves higher order spatial accuracy using a narrow stencil, it suffers from the same problems as the Yee scheme and its straightforward extensions discussed above scheme, i.e., difficulties with accurately representing boundaries and material interfaces. The implicit nature of the compact scheme, however, makes it difficult to utilize local remedies as for the explicit scheme since any such local adjustment has a global impact. Initial work in this direction is reported in [119], in which the compact stencil is locally modified to allow for a non-conforming Dirichlet boundary condition as required in the two-dimensional TM-form, Eq.(13). The scheme, however, requires one to physically moves the grid points, thus introducing severe stiffness for cases where the boundary is close to a grid-point of the equidistant grid. More general types of boundary conditions, e.g., magnetic boundaries, are not treated. In related work [117, 135] the problem of material interfaces is addressed by using high-order smooth approximations to material parameters. While this visually improves on the accuracy, a rigorous analysis was not done and the computational results restricted to cases where all field components are continuous.

Using a nonstaggered grid, it is proposed in [106] to terminate the compact stencils with explicit schemes. While it is found experimentally that one needs to use a filter to avoid instabilities, full three-dimensional scattering results have been reported. The accuracy of this approach is not known.

The formulation of the compact schemes, leading to the operators P and Q given above, is done with accuracy in mind. The equally important question of stability must then be addressed subsequently. This is known to be a task of considerably complexity and often requires special techniques to impose boundary conditions, see e.g. [12, 13].

The complementary approach to this is the direct construction of stable high-order schemes. Such schemes, known as summation-by-parts (SBP) schemes, were originally proposed in [81], and developed further in [113, 96, 97]. The discrete operators, P and Q, are derived to mimic the integration-by-parts property of the divergence operator, leading to the conditions that P be symmetric, positive definite, and Q almost skew-symmetric, i.e., $\mathrm{Q}+\mathrm{Q}^T = \mathrm{diag}[-1,0...,0,1]$. Both P and Q are typically banded, with examples given in [81, 113].

Imposing boundary conditions in this type of schemes is a bit more complex as modifying the operators directly may destroy the SBP-property. The standard approach is thus to impose the conditions weakly through a simultaneous-approximation-term (SAT) as

$$\frac{du}{dx}\ ,\ u(1)=g \quad \Rightarrow \mathrm{P}^{-1}\frac{d\boldsymbol{u}}{dx} = \mathrm{Q}u - \mathrm{T}\left[u(1)-g\right] \quad .$$

Here $\mathrm{T} = \mathrm{diag}[0,0....,0,\tau]$ where $\tau \geq 1$ ensures stability. Since the boundary conditions are imposed as an additional term, more complex boundary operators can be imposed in a similar way.

SBP schemes for Maxwell's equations are discussed in [95], showing the expected accuracy and stability for the two-dimensional TE-form, Eq.(12), in simple grid-conforming geometries. The scheme preserves divergence in regions of homogeneous materials. Treatment of material interfaces is done in a way similar to that discussed

in Sec. 4.1, i.e., by treating the different regions separately and using the physical jump-conditions to connect the regions.

As for the compact scheme, the SBP methods have problems treating geometrically complex problems due to the implicit nature of the schemes. Furthermore, the SBP property is delicate and even the use of simple curvilinear mappings may destroy this property, thus ruining the stability. It is worth while mentioning that a 2nd order accurate scheme, using the SAT-approach, for arbitrary embedded metallic boundaries has been proposed in [1]. It is conceivable that similar ideas can be adapted to a 4th order scheme, although the analysis promises to be complex.

4.3. Fictitious and Overlapping Grid Methods

In the straightforward extensions of the Yee scheme discussed in Sec. 4.1 it was proposed to use extrapolations and strongly enforce the jump-conditions. Methods, taking this approach one step further by using the equation repeatedly at the interface also, were recently proposed in [25, 26] for one- and two-dimensional problems in electromagnetics. Similar ideas have been proposed previously in the context of acoustics and elasticity but apparently never implemented [136, 137].

These schemes employ a standard high-order explicit finite difference scheme on a nonstaggered grid in regions with homogeneous materials. Close to boundaries and interfaces, however, a different procedure is taken, much in the spirit of Sec. 4.1, albeit using a different approach.

To illustrate the central idea, consider again the one-dimensional Maxwell's equations, Eq.(11), on the form

$$\frac{\partial \boldsymbol{q}}{\partial t} = \mathrm{A}(x)\frac{\partial \boldsymbol{q}}{\partial x} \quad , \quad \boldsymbol{q} = \begin{bmatrix} E^z \\ H^z \end{bmatrix} \quad , \quad \mathrm{A} = \begin{bmatrix} 0 & \varepsilon_r^{-1}(x) \\ \mu_r^{-1}(x) & 0 \end{bmatrix} \quad .$$

For simplicity we restrict the attention to the case of a material interface at $x = x_{\mathrm{mat}}$ across which we have that $\boldsymbol{q}$ is continuous, i.e.,

$$\boldsymbol{q}(x_{\mathrm{mat}}^-, t) = \boldsymbol{q}(x_{\mathrm{mat}}^+, t) \quad .$$

Using the equation themselves, however, we also have that

$$\mathrm{A}(x_{\mathrm{mat}}^-)\boldsymbol{q}^{(1)}(x_{\mathrm{mat}}^-, t) = \mathrm{A}(x_{\mathrm{mat}}^+)\boldsymbol{q}^{(1)}(x_{\mathrm{mat}}^+, t) \quad , \tag{19}$$

i.e., we have conditions on the first spatial derivatives, $\boldsymbol{q}^{(1)}$, of $\boldsymbol{q}$ across the interface. One can of course repeat this argument as often as needed to obtain

$$\mathrm{A}(x_{\mathrm{mat}}^-)^p\boldsymbol{q}^{(p)}(x_{\mathrm{mat}}^-, t) = \mathrm{A}(x_{\mathrm{mat}}^+)^p\boldsymbol{q}^{(p)}(x_{\mathrm{mat}}^+, t) \quad .$$

We assume that we solve Maxwell's equations on a simple equidistant grid, x_j, although it could also be staggered.

Consider the situation in Fig. 5, where the two regions of different materials are separated at x_{mat} which do not have to coincide with a grid point. Everywhere away from the interface, we shall use whatever explicit finite-difference preferred, cf. Sec. 4.1. To update the values of $\boldsymbol{q}$ at points close to the interface, e.g., $x_N^{(1)}$

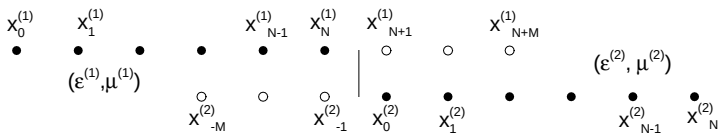

FIG. 5. Illustration of ghost grids and numbering used in overlapping grid methods.

and $x_0^{(2)}$, we shall assume the existence of ghost-points, $x_{N+m}^{(1)}$ and $x_{-m}^{(2)}$, $m = 1..M$. Clearly, if the values of $\boldsymbol{q}$ were known at these points, one could update $\boldsymbol{q}$ at $x_N^{(1)}$ and $x_0^{(2)}$ using standard finite difference stencils.

We can, however, use the additional constraints, Eq.(19). One can approximate the one-sided derivatives as central differences

$$\boldsymbol{q}^{(p)}(x_{\text{mat}}^-) \simeq \sum_{j=N-M}^{N+M} v_j^{(p)} \boldsymbol{q}(x_j^{(1)}) \ , \ \boldsymbol{q}^{(p)}(x_{\text{mat}}^+) \simeq \sum_{j=-M}^{M} w_j^{(p)} \boldsymbol{q}(x_j^{(2)}) \ ,$$

where $v_j^{(p)}$ are the weights corresponding to computing derivatives using values left of the interface and $w_j^{(p)}$ using values from right of the interface. These can be found on closed form using Lagrange polynomials as in Sec. 4.1, or computed as discussed in [32]. Note that $p = 0$ corresponds to interpolation at x_{mat}.

There are a total of 2M unknown ghost-values, implying that we will need 2M constraints, Eq.(19), to recover these, typically resulting in a scheme of $\mathcal{O}(h^{2M})$ close to the interface, e.g., if a 4th order scheme is used in the interior, one needs 4 additional constraints to compute the 4 ghost values. Clearly, one can initialize all operators in a pre-processing stage as they depend on the weights only which again depends on the order of accuracy and position of interface. In the original work [25] this is taken to the limit by using maximal accuracy, i.e., a global spectral method, everywhere in each region of homogeneous material. This requires additional attention to positions of the grids close to the interfaces. We refer to [25] for the details.

To illustrate the performance of such an approach we show in Fig. 6 computational results obtained by solving the one-dimensional Maxwell's equations, Eq.(11). The problem is very similar to that considered earlier, although the domain is considered periodic rather than truncated by a metallic cavity and the initial condition is a Gaussian pulse in one domain. As the pulse propagates, it experiences multiple reflections and transmissions at the interfaces. The figure clearly illustrates the importance of correctly treating the material interfaces, in particular for problems requiring long time integration.

In [26] these ideas are extended to two-dimensional problems, simplified by assuming that the material interface can be smoothly mapped to align with a coordinate axis. In that case, the modifications needed to maintain accuracy remains essentially one-dimensional. The only additional complication is that deriving conditions, Eq.(19), for the multi-dimensional case introduces cross-derivatives

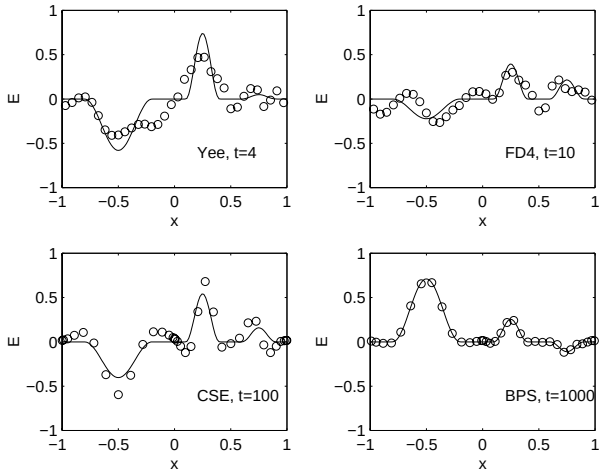

FIG. 6. Computational results for a pulse undergoing multiple reflections at a material interface ($\varepsilon_r^{(1)} = 1.0$ and $\varepsilon_r^{(2)} = 4.0$ as obtained using different schemes. The computations are terminated where the results are visibly bad. While the Yee scheme quickly looses the correct the solution, also the standard 4th order finite difference performs poorly after only 10 periods. The overlapping scheme (BPS) uses a global scheme in each domain and performs very well after long time. The results marked CSE are obtained using a spectral multi-domain scheme (Sec. 5.2). The figure is courtesy of T. Driscoll and B. Fornberg.

for $M > 1$. Thus, only one ghost-point in used and the stencils become one-sided as needed.

For smooth interfaces, it is proposed to used an overlapping patch or grid, conforming to the interface and employ the ghost-point approach to update the solution at the interface. The solution at the patch is smoothly blended, using a partition-of-unity approach, with the solution at an underlying equidistant grid to obtain the global solution. An example of a grid is shown in Fig. 7. Computational examples on this and other simple grids can be found in [26].

While the use of fictitious (or ghost-) points has shown promise, many issues remain open, in particular related to the extension of such techniques to more general two- and three-dimensional problems, as well as problems involving non-smooth geometries. Furthermore, the stability of these methods has not been analyzed.

5. SPECTRAL METHODS

The classical phase error analysis, Sec. 3, as well as the results discussed above suggest advantages in going to even higher order accurate schemes to further reduce work and memory requirements while maintaining the accuracy.

A straightforward execution of such ideas, however, introduces issues related to computational efficiency when computing with very wide stencils, as well as difficulties associated with finite computational domains and complex geometries.

In the following we shall discuss techniques proposed to overcome these concerns while maintaining the accuracy and efficiency of the very high-order schemes.

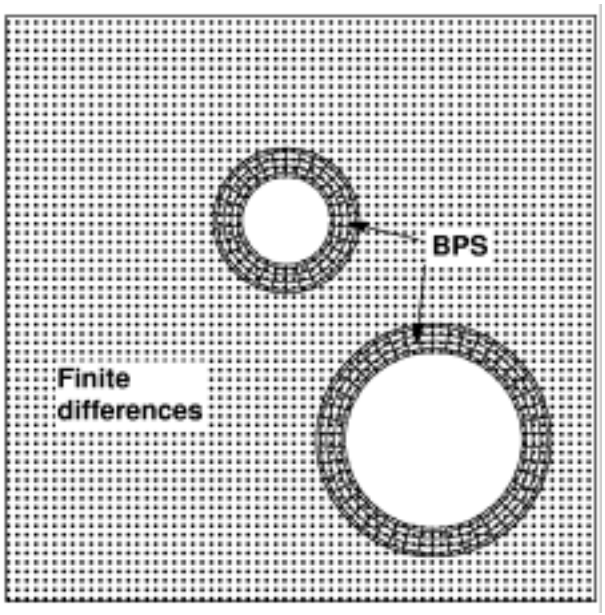

FIG. 7. Example of a overlapping grid approach, used to extend the ghost-point approach to two-dimensional problems. The figure is courtesy of T. Driscoll and B. Fornberg.

5.1. Global Methods

If we maintain the typical scenario when using a high-order finite difference scheme and assume that we have a simple equidistant grid, one can imagine using a stencil spanning the whole computational grid, i.e., a global method. The problems with this straightforward approach are several, e.g., the computational cost and the development of stable and accurate means of dealing with the ends of the computational domain.

The benefits of overcoming such problems are, however, quite substantial as can be realized by recalling Eq.(15). Letting m increase we see that one could expect that the required number of points per wavelength becomes independent of accuracy and integration time. In other words, once this requirement is fulfilled, the scheme solves the wave propagation problem exactly. As was shown in [80], this intuition holds with the requirement being only two points per wavelength.

One way of overcoming some of the problems to harvest the advantages of using a global scheme was first proposed in [86] in the context of Maxwell's equations. At first, one assumes that the solution is spatially periodic to overcome the problems with terminating the computational domain and designing large, one-sided stencils. A further advantage of this assumption is the well known result [80, 31] that the infinite order finite difference scheme for a periodic problem is nothing else than a pseudospectral Fourier method. In other words, the $\mathcal{O}(N^2)$ computation of derivatives

$$\left.\frac{du}{dx}\right|_{x_j} = \sum_{k=0}^{N} \mathrm{D}_{jk} u(x_k) \quad ,$$

where D is a dense differentiation matrix, can be done through a Fourier series as

$$\left.\frac{du}{dx}\right|_{x_j} = \sum_{n=0}^{N} (in)\tilde{u}_n \exp(inx_j) \quad , \quad \tilde{u}_n = \frac{1}{N+1}\sum_{j=0}^{N} u(x_j)\exp(-inx_j) \quad ,$$

where $x_j = 2\pi j/(N+1)$ represent the equidistant grid points. The benefit of this formulation is that both summations can be done in $\mathcal{O}(N \log N)$ operations by using the Fast Fourier Transform.

The assumption of periodic solutions may, at first, seem to severely limit the use of such methods. The central idea in [86], however, was to surround the computational domain with an absorbing layer, a perfectly matched layer (PML) [4, 5, 117]. Assuming that the absorption of waves is sufficiently efficient, the solution on the outer boundary almost vanishes, thus achieving the periodicity. This approach has been used successfully to model large scale three-dimensional wave-propagation and scattering problems, see e.g. [87], using a little as 2 points per wavelength. See also [85] for a comparison between PSTD and classical Yee schemes for scattering problems.

As efficient and simple as this approach is, it has a number of limitations. The need to completely surround the computational problem with an absorbing layer essentially limits the attention to open space problems, although one could deal with simple interior problems by choosing a particular basis. The most severe limitation is, however, the very same as that of the simple extensions of the Yee scheme, i.e., an inability to handle interior interfaces and boundaries.

This is emphasized by the simple approximation result that [11]

$$\|u - u_N\| \leq N^{-q}\|u^{(q)}\| \quad ,$$

where u_N represents the Fourier approximation of u, and $u^{(q)}$ reflects the q'th derivative. Clearly, if u is very smooth, i.e., $\|u^{(q)}\|$ is bounded for high values of q, the convergence is very fast and the function is well represented with only few points per wavelength. Unfortunately, it is the other limit that is relevant regarding the solution of Maxwell's equations for problems involving interior boundaries and interfaces. In such cases a best case scenario is that $q \leq 1$, i.e., one can not expect better than local first and global second order accuracy even for problems where material interfaces are aligned with the grid. For curvilinear interfaces, where the fields may be discontinuous, the situation is worse and the combined impact the lack of smoothness and staircasing will be significant.

Due to the global nature of the approximation and the need to use the Fast Fourier Transform for computational efficiency, it is difficult to see how to overcome these shortcomings, e.g., straightforward local modifications of the stencils as for the finite difference schemes are not possible, and the benefits of using local smooth mappings is limited for problems with even moderate geometric complexity [11].

5.2. Multi-Domain Formulations

The most significant restriction of the global methods discussed is the inability to correctly deal with problems in complex geometries. While several techniques were discussed for the 4th order finite difference schemes in Sec. 4, these methods are only

now emerging and much work is still needed. Furthermore, it is unclear whether such techniques allows one to formulate schemes beyond 4th order accuracy.

Thus, it seems natural to consider alternatives, allowing one to maintain global high-order accuracy even in situations with geometric complexity. The main observation to make is that the efficiency of a high-order method is closely related to the smoothness of the solution. When internal interfaces and boundaries are present, the global smoothness is generally reduced and one does not benefit as much from using high-order methods as one could expect. However, the solution often remains smooth in regions of smoothly varying or constant material parameters, with these regions being separated by well defined geometric features.

The only practical way to take advantage of this is to leave the simple equidistant grids behind and consider the formulation of high-order accurate schemes using body-conforming grids. For general geometries, one can not hope, however, to accomplish this with simple globally mapped grids but must consider a multi-element or multi-domain formulation in which the computational domain is composed as a union of non-overlapping elements.

Such an approach introduces a couple of issues that needs careful attention, e.g., how does one compute derivatives at the individual elements to high order and how does one connect the local element wise solutions to form the global solution in a stable manner. The resolution of the questions has been the topic of recent research [71, 129, 130, 131] pawing the way for high-order accurate scheme without the problems of the finite-difference scheme. In the following we shall discuss the elements of this formulation in some more detail.

5.2.1. The Local Scheme

We shall assume that the computational domain, Ω, is split into K non-overlapping elements. This is done in a way such that interfaces are aligned with the geometry, i.e., returning to the one-dimensional cavity problem discussed previously, a straightforward splitting is into two elements, corresponding to each of the two regions of different materials.

As we will now need to represent solutions and derivatives of solutions on finite domains, it is well known that we must abandon the use of a simple equidistant grid in each domain. Indeed, we must use a grid that clusters close to the ends of the element. A suitable choice could be the mapped Chebyshev Gauss Lobatto nodes (see e.g. [31, 39])

$$i = 0..N \ : \ x_i = a + \frac{1-\cos(i\pi/N)}{2}(b-a) \ ,$$

where the element spans $[a, b]$ and $N + 1$ are the number of grid points in the domain.

Following the basic approach of a finite difference method, one can now form elementwise Lagrange interpolation polynomials on the form

$$l_i(x) = \frac{(-1)^{N+1+j}(1-\xi(x)^2)T_N'(\xi(x))}{N^2 c_i(\xi(x)-\xi(x_i))} \ ,$$

where $T_n(\xi) = \cos(n \arccos \xi)$ represents the n'th order Chebyshev polynomial, $c_0 = c_N = 2$, and $c_i = 1$ otherwise. The scaled variable, $\xi(x)$, is given as

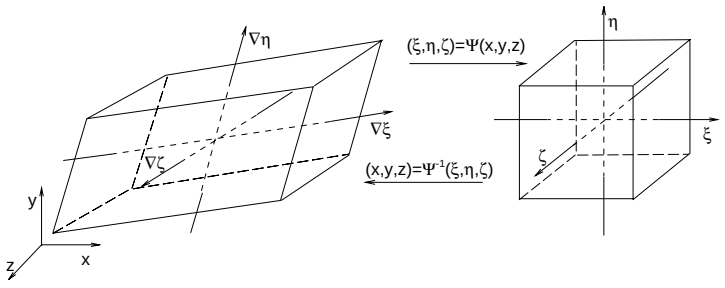

FIG. 8. Illustration of the curvilinear mapping used in the multidomain formulation

$$\xi(x) = 2\frac{x-a}{b-a} - 1 \quad .$$

With this, we can represent the local element wise solutions as

$$u_N(x) = \sum_{i=0}^{N} u(x_i) l_i(x) \quad ,$$

and compute the pointwise derivatives in a similar fashion as for finite difference schemes, i.e., by a matrix-multiply as

$$\left.\frac{du}{dx}\right|_{x_j} \simeq \left.\frac{du_N}{dx}\right|_{x_j} = \sum_{i=0}^{N} u(x_i) \mathrm{D}_{ji} \quad ,$$

where the differentiation matrix, D, has the entries [39]

$$\mathrm{D}_{ji} = \frac{dl_i(x_j)}{dx} = \begin{cases} -\frac{2N^2+1}{6} & i = j = 0 \\ \frac{c_j}{c_i}\frac{(-1)^{i+j}}{x_j - x_i} & i \neq j \\ -\frac{x_i}{2(1-x_i^2)} & 0 < i = j < N \\ \frac{2N^2+1}{6} & i = j = N \end{cases} \quad .$$

Thus, with this we can represent solutions and evaluate derivatives with spectral accuracy, provided the solution is sufficiently smooth on the element [11].

The extension of this to multidimensional problems utilizes tensor products, i.e., a two dimensional function is represented as

$$u_N(x,y) = \sum_{i=0}^{N}\sum_{j=0}^{N} u(x_i, y_j) l_i(x) l_j(y) \quad ,$$

and likewise for a three-dimensional field. The computation of derivatives follows the approach above.

While this allows the accurate computation of spatial derivatives, it also assumes that $u(x,y)$ is defined on a rectangular grid. This restriction we can overcome by

considering a curvilinear representation. In other words, we assume the existence of a smooth non-singular mapping function, Ψ, relating the (x, y, z)-coordinate system to the general curvilinear coordinate system (ξ, η, ζ) as illustrated in Fig. 8. To establish a one to one correspondence between the unit cube, $\mathsf{I} \subset \mathsf{R}^3$, and the general curvilinear hexahedral, D, we construct the local map for each sub-domain using transfinite blending functions [38]. We refer to [48] for a thorough account of this procedure within the present context. Thus, we have Cartesian coordinates, $(x, y, z) \in \mathsf{D}$, and the general curvilinear coordinates, $(\xi, \eta, \zeta) \in \mathsf{I}$.

On curvilinear form, Maxwell's equations take the form

$$\mathrm{Q}\frac{\partial \boldsymbol{q}}{\partial t} + \mathrm{A}(\nabla\xi)\frac{\partial \boldsymbol{q}}{\partial \xi} + \mathrm{A}(\nabla\eta)\frac{\partial \boldsymbol{q}}{\partial \eta} + \mathrm{A}(\nabla\zeta)\frac{\partial \boldsymbol{q}}{\partial \zeta} = 0 \quad , \tag{20}$$

with the state vector, $\boldsymbol{q} = (\boldsymbol{E}, \boldsymbol{H})^T$, and the material matrix, $\mathrm{Q} = \mathrm{diag}(\varepsilon_r, \varepsilon_r, \varepsilon_r, \mu_r, \mu_r, \mu_r)$. The general operator, $\mathrm{A}(\boldsymbol{n})$, depending on the local normal vector, $\boldsymbol{n} = (n_x, n_y, n_z)$, obtained from the metric through the mapping, Ψ, is given as

$$\mathrm{A}(\boldsymbol{n}) = \begin{bmatrix} 0 & 0 & 0 & 0 & n_z & -n_y \\ 0 & 0 & 0 & -n_z & 0 & n_x \\ 0 & 0 & 0 & n_y & -n_x & 0 \\ 0 & -n_z & n_y & 0 & 0 & 0 \\ n_z & 0 & -n_x & 0 & 0 & 0 \\ -n_y & n_x & 0 & 0 & 0 & 0 \end{bmatrix} \quad .$$

We show in Fig. 9 as an example a simple two-dimensional holographic waveguide coupler and the geometry conforming multi-domain grid. The mapped Chebyshev grid in each element allows accurate computation of derivatives while the body fitted grid ensures that the solution is smooth inside each element, hence taking advantage of the accuracy of the high order scheme.

5.2.2. Connecting the Elements

Having the ability to accurately and efficiently compute derivatives in a general curvilinear hexahedral and, thus, solve Maxwell's equations in such a domain, we must now focus on the question of how to assemble these local solutions to recover a global solution in a time-stable and accurate manner. Clearly, care has to be exercise here as Maxwell's equations supports counter propagating waves, consisting of both electric and magnetic fields, i.e., one can not simply enforce continuity across the interfaces.

The central observation to make, utilized in the context gasdynamics also [76, 77, 48], is that Maxwell's equations, written as in Eq.(20), is a strongly hyperbolic system. In other words, we can diagonalize the matrix $\mathrm{Q}^{-1}\mathrm{A}(\boldsymbol{n})$ as

$$\mathrm{S}^T\mathrm{Q}^{-1}\mathrm{A}(\boldsymbol{n})\mathrm{S} = c_r|\boldsymbol{n}| \begin{bmatrix} -1 & 0 & 0 & 0 & 0 & 0 \\ 0 & -1 & 0 & 0 & 0 & 0 \\ 0 & 0 & 0 & 0 & 0 & 0 \\ 0 & 0 & 0 & 0 & 0 & 0 \\ 0 & 0 & 0 & 0 & 1 & 0 \\ 0 & 0 & 0 & 0 & 0 & 1 \end{bmatrix} \quad .$$

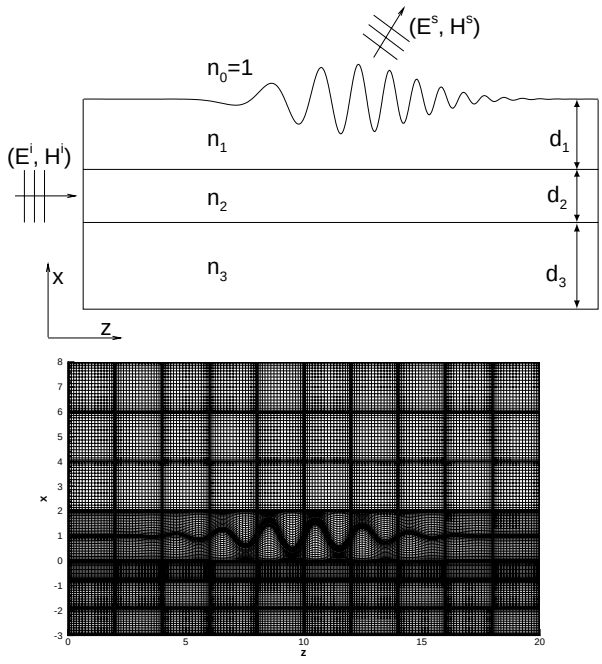

FIG. 9. On top we show a sketch of a diffractive waveguide coupler and below a multi-domain spectral grid used to model such a geometry.

Here $c_r = (\mu_r \varepsilon_r)^{-1/2}$ is the local speed of light and $|\boldsymbol{n}|$ the length of the normal. The entries of S can be found in [131] and a simplified two-dimensional form in [129].

Let us first consider the case where two neighboring elements can be assumed to have smoothly varying materials. If we compute the characteristic functions, $\boldsymbol{R} = \mathrm{S}^T \boldsymbol{q}$, then the entries in the above diagonal matrix tell exactly how these functions are propagating, e.g., R_1 and R_2 propagates antiparallel to $\boldsymbol{n}$, R_5 and R_6 propagates parallel to $\boldsymbol{n}$, while R_3 and R_4 signifies a non-propagating DC component. With this one knows exactly which information propagates where at any point of the boundary of the an element. Furthermore, what leaves one element, i.e., R_5 and R_6, must correspond exactly to what enters the neighboring element through R_1 and R_2. Thus, R_5 and R_6 provides the boundary conditions needed to solve the neighboring solution. The non-propagating characteristic waves can be required to be continuous.

At a material interface, the situation can be dealt with in two different ways. One can either rescale the characteristic variables to account for the abrupt change in the materials or one can abandon the characteristic variables and simply enforce the physical jump-conditions on the fields, e.g., continuity of the tangential fields.

5.2.3. A Few Examples

To illustrate the performance of the multi-domain spectral scheme discussed in the above, let us consider a few examples.

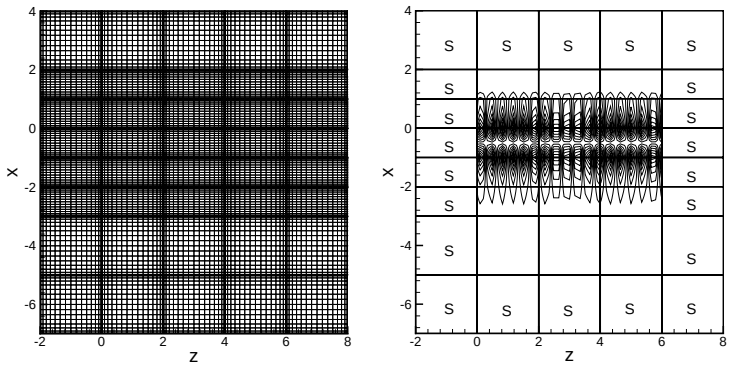

FIG. 10. Illustration of plane waveguide test case. The grid shows the general layout with the high-index waveguide just below $x = 0$ and $N = 16$ modes in each domain. On the right is a snapshot of the H^z component at an arbitrary time illustrating the total field region as well as the surrounding scattered field region (marked by an S).

As a first one, consider simple two-dimensional TM polarized wave propagation in a planar multi layer waveguide, as illustrated in Fig. 10. The waveguide is 6λ long waveguide where the core layer has a thickness of $d_2 = \lambda$ and an index of refraction $n_2 = 1.45$, the cladding layers both have $n_1 = n_3 = 1.4$, while the thickness of the two cladding layers are $d_1 = \lambda$, and $d_3 = 4\lambda$, respectively. The total field region, in which the computation is conducted, as well as the surrounding scattered field region with the absorbing layers are shown in Fig. 10. A 4th order Runge-Kutta scheme is used to advance in time and a PML to truncate the computational domain (see [51] for details).

TABLE 1
Error in the computation of the plane waveguide solution at $t = 10$.

N	N_{ppw}	Δt	$L_\infty(H^z)$	$L_\infty(H^x)$	$L_\infty(E^y)$
12	4.3	3.1E-2	5.0E-2	3.6E-1	2.5E-1
16	5.7	2.1E-2	1.1E-3	8.5E-3	6.0E-3
20	7.1	1.4E-2	6.9E-6	4.8E-5	3.9E-5
24	8.5	1.1E-2	2.2E-6	1.5E-5	1.1E-5

As a validation of the expected spectral accuracy, we list in Table 1 the global L_∞ error measured after 10 periods. Not only do we find spectral convergence but also that less than 6 points per wavelength (N_{ppw}) yields an acceptable accuracy for many applications.

As a second example, considered in more detail in [130], we consider scattering by an axisymmetric three-dimensional metallic scatterer, in this case a rocket-shaped nonsmooth object. In Fig. 11 we illustrate the body-conforming grid and Fig. 12 shows a comparison of the bistatic radar-cross-section (RCS) for different polar-

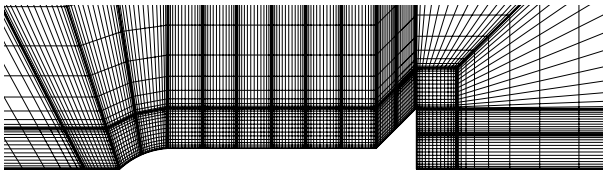

FIG. 11. Typical multi-domain grid for the solution of scattering by a three-dimensional axisymmetric missile.

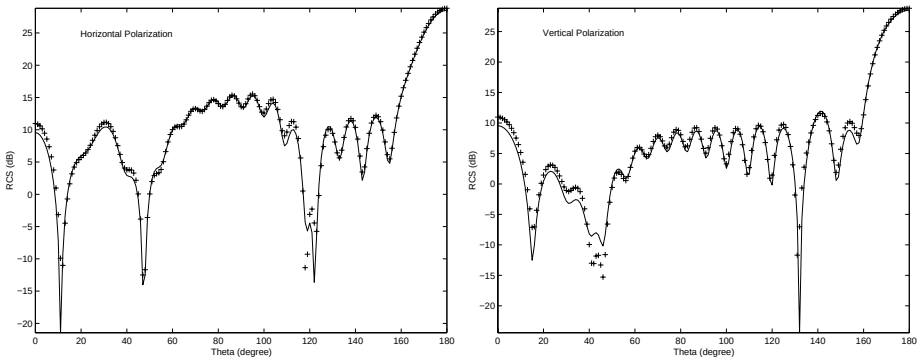

FIG. 12. On the left is shown the RCS(θ,0) for a missile subject to axial illumination by a horizontally polarized plane wave and one the right the results under vertical polarization. A reference solution is marked by "+".

izations as compared with results obtained using a contemporary integral equation solver. The results are essentially identical.

As a final example, let us consider a three-dimensional problem, in this case plane wave scattering by a $ka = 5.3$ di-electric sphere. The sphere consists of a nonmagnetic material with $\epsilon_r = 3$ [131]. Excellent results for the radar-cross-section, obtained with about 8 points per wavelength on the surface of the sphere, is shown in Fig. 13 along with a segment of the grid.

The multidomain scheme has by now been implemented and tested for a variety of problems, including three-dimensional waveguide and diffractive optics [23], quasi-three-dimensional [138] and fully three-dimensional scattering [131, 139], and propagation in lossy media [131, 28]. Excellent parallel performance is demonstrated in [23].

As flexible and versatile as the multi-domain spectral approach is, these benefits do come at a price, most notably the problems of constructing a high-order body conforming block structured grid. Furthermore, for highly curved elements one has to be careful to avoid instabilities caused by aliasing, and to resolve both the solution and the geometry sufficiently accurate. For nontrivial problems is it often advantageous to use a high-order filter [129, 51, 39] to improve robustness, although care has to be taken not to adversely impact the accuracy.

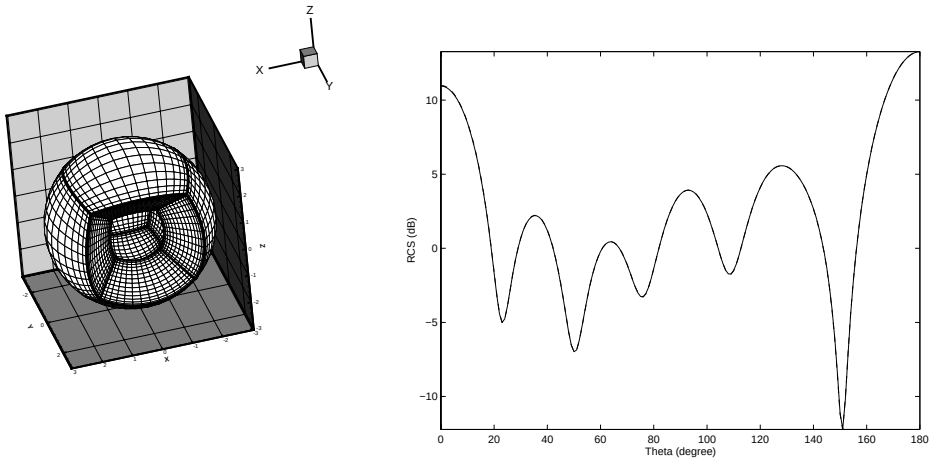

FIG. 13. On the left is shown an example of a three-dimensional curvilinear grid for scattering by a $ka = 5.3$ dielectric sphere with $\epsilon_r = 3$, and $\mu_r = 1$. On the right is shown the computed bistatic radar-cross-section (RCS) (full lines) as compared with the exact solution (dashed line) computed using a Mie series.

6. HIGH-ORDER FINITE VOLUME SCHEMES

The need for geometric flexibility is shared with many other diciplines and it is tempting to try and take advantage of such related developments. Given the wave nature of the solutions, it is natural to turn the attention towards methods from gasdynamic where one of the most remarkable and successful developments has been the finite volume methods, combining the geometric flexibility of an unstructured grid with the ability to handle nonsmooth solutions.

The finite volume method is based on a discretization of the conservation law

$$\frac{\partial u}{\partial t} + \nabla \cdot f(u) = 0 \ ,$$

where u is the solution and $f(u)$ represents a flux, often of a nonlinear character. Introducing a grid with grid points, $\boldsymbol{x}_i \in \Omega$, centered in the individual control volumes, D, we integrate over the control volume and invoke Gauss' theorem to recover

$$A(\mathsf{D})\frac{d\overline{u}_i}{dt} + \oint_{\partial \mathsf{D}} \hat{\boldsymbol{n}} \cdot f(u)\, d\boldsymbol{x} = 0 \ ,$$

where $A(\mathsf{D})$ represents the area/volume of D, $\overline{u}_i$ the cell-averaged solution value, i.e.,

$$\overline{u} = \int_{\mathsf{D}} u(\boldsymbol{x})\, d\boldsymbol{x} \ , \tag{21}$$

and $\hat{\boldsymbol{n}}$ an outward pointing normal vector at the boundary of D.

To put this into the context of Maxwell's equations, one needs only realize that Eqs.(7)-(8) can be written as

$$\mathrm{Q}\frac{\partial \boldsymbol{q}}{\partial t} + \nabla \cdot \boldsymbol{F}(\boldsymbol{q}) = \boldsymbol{S} \quad , \tag{22}$$

where Q represents the materials, $\boldsymbol{q} = [\boldsymbol{E}, \boldsymbol{H}]^T$, and the flux, $\boldsymbol{F} = [\boldsymbol{F}_1, \boldsymbol{F}_2, \boldsymbol{F}_3]^T$ has the components

$$\boldsymbol{F}_i(\boldsymbol{q}) = \begin{bmatrix} -\hat{\boldsymbol{e}}_i \times \boldsymbol{H} \\ \hat{\boldsymbol{e}}_i \times \boldsymbol{E} \end{bmatrix} \quad , \tag{23}$$

where $\hat{\boldsymbol{e}}_\alpha$, $\alpha = (x, y, z)$, represents the three Cartesian unit vectors.

The close connection between gas dynamics and electromagnetics has been explored in a series of papers [108, 107, 109, 33, 110, 35], devoted to the development of high-order accurate finite volume methods on structured and locally orthogonal, but unstructured grids.

So far, everything in the above discussion remains exact. However, as we only have cell-centered solution values, $\overline{u}_i$, evaluating the fluxes, $f(u)$, which depend on the solution, along the circumference of the element can not be done in a straightforward manner. This problem, being one of reconstruction in contrast to the approximation of derivatives as discussed so far, is at the heart of the finite volume method and is where the approximation enters.

As shown in [47], if one can evaluate the local fluxes to $\mathcal{O}(h^n)$, then the truncation error of the cell averaged solutions, $\overline{u}$, are also $\mathcal{O}(h^n)$, i.e., we can focus on the scheme for reconstructing the local fluxes.

Borrowing directly from the successes in computational fluid dynamics, one could again use the notion of characteristic waves, discussed in Sec. 5.2, and form the edge based solution by upwinding from both sides of the edge. Assuming for simplicity a locally Cartesian grid, as done in [108, 33], one expresses the edge fluxes as

$$f(x_{i+1/2}) = F(u^L, u^R) = F^+(u^L) + F^-(u^R) \quad ,$$

where $F^+(u)$ and $F^-(u)$ corresponds to the downwind, i.e., positive eigenvalues, and $F^+(u)$ to the upwind, i.e., negative eigenvalues, components of the characteristic waves discussed in Sec.5.2. This flux splitting is non unique with suggestions given in [107, 109] in a general curvilinear formulation.

Given the linearity of the fluxes, the accuracy of the reconstructed solution values, i.e., u^L and u^R reconstructed from the left and right of edge, determines the overall accuracy. Assuming a locally equidistant grid, it is proposed in [108, 33] to use the MUSCL fluxes

$$u^L_{i+1/2} = \left(1 + \frac{1}{6}\left(\nabla + 2\Delta\right)\right)\overline{u}_i \quad , \quad u^R_{i+1/2} = \left(1 - \frac{1}{6}\left(2\nabla - \Delta\right)\right)\overline{u}_{i+1} \quad ,$$

where $\nabla = \mathrm{E}_0 - \mathrm{E}_{-1}$ and $\Delta = \mathrm{E}_1 - \mathrm{E}_0$ where E_i is the shift-operator defined in Eq.(14). This approach is based on local Taylor expansions and is accurate to $\mathcal{O}(h^3)$, i.e., the scheme can be expected to be third order accurate on a locally uniform grid. Alternatives to the upwinded reconstructions are discussed in [108].

The numerical dispersion and grid-anisotropy for this method is discussed in [107, 109, 33] and simulations using curvilinear, orthogonal grids are shown in [110].

As discussed above, at the heart of the finite volume scheme is the need to reconstruct the local solution, using only cell averaged values. The approach discussed above is essentially limited to 3rd order accuracy by the MUSCL flux. An alternative is discussed in [33] and introduce the new one-dimensional variable

$$V(x) = \int_0^x u(s)\,ds \quad , \quad \frac{dV}{dx} = u(x) \quad ,$$

i.e., if one can evaluate the pointwise derivative of $V(x)$ accurately, one can reconstruct the local pointwise value of $u(x)$ accurately. However, from the definition of $\overline{u}$, Eq.(21), it follows directly that

$$V_{1/2} = 0 \quad , \quad V_{i+1/2} = V_{i-1/2} + h\overline{u}_i \quad ,$$

assuming a simple one-dimensional equidistant grid. The extension to multiple dimensions involves tensor-product grids. With the grid function $V_{i+1/2}$ computed, we can now use any of the finite difference technique discussed in Sec. 4 to compute the local derivative of $V_{i+1/2}$ to recover $u_{i+1/2}$ and, consequently, the local flux. Clearly, the order of this approach will depend on the scheme chosen to evaluate the derivative of $V(x)$. In [33, 35, 34] it is advocated to use an implicit compact stencil, similar to the ones discussed in Sec. 4.2. Other techniques discussed in Sec. 4 could equally well be used. Dispersion errors of the compact schemes are discussed in [33] and errors associated with stretched grids are addressed in [35]. Dispersion optimized compact reconstructions are introduced in [34].

As appealing and simple as the finite volume schemes are, they suffer from shortcoming similar to those of the finite difference schemes discussed previously, e.g., an inability to accurately deal with material interfaces and complex geometries. This is caused by the high-order reconstructions essentially being based on logically Cartesian grids. Furthermore, the compact reconstruction essentially assumes local smoothness of the solutions, which may not be the case across material interfaces. Exploiting embedding techniques may be a way of overcoming this.

7. FINITE ELEMENT SCHEMES

Through the above discussions it has become clear that the need to accurately and systematically handle geometric complex problems is perhaps the most significant challenge when developing new methods. This realization is, however, not unique to electromagnetics and much work has been done to address this problem in other areas of computational science.

The ability to effectively and accurately handle this problems remains one of the main reasons for the remarkable success of finite element methods in solid and fluid mechanics (see [63] and references therein), leading to its widespread use and availability of numerous commercial software environments.

The use of finite elements for solving Maxwell's equations has, however, been relatively slow, in spite of early efforts [111, 15, 112]. This can be attributed partly to the need to address numerous technical questions, e.g., element types,

equation form and correct variational statements, and partly to the failure of the most straightforward formulations. The success of the finite difference methods for many problems combined with it simplicity also made the finite element formulation less attractive.

With the growing need to solve geometrically complex large scale problems, the last last decade has seen a increasing interest in the flexibility offered by finite element schemes, although most of the developments has been for problems formulated in the frequency domain [69, 120].

Only more recently has finite element schemes for the time-domain solution of Maxwell's equations received more attention [82], focusing almost exclusively on low order formulations. The development of high-order accurate finite element methods for the time-domain solution of Maxwell's equation remains an emerging field at this point in time, although some of the results we shall discuss in the following show illustrate its potential.

7.1. Continuous Finite Element Techniques

When formulating a finite element scheme for solving Maxwell's equations, one encounters a number of questions, the first one being on which form to consider the equations themselves.

On one hand one could consider solving the equations on first order form, Eq.(3),

$$\varepsilon_r \frac{\partial \boldsymbol{E}}{\partial t} = \nabla \times \boldsymbol{H} + \boldsymbol{J} \quad , \quad \mu_r \frac{\partial \boldsymbol{H}}{\partial t} = -\nabla \times \boldsymbol{E} \quad . \tag{24}$$

The treatment of these first order non-self-adjoint operators is, however, often a source of significant problems in classical finite element formulations.

An attractive alternative, and one that is most often used, is obtained by combining the two first order equations to recover the selfadjoint curl-curl form

$$\varepsilon_r \frac{\partial^2 \boldsymbol{E}}{\partial t^2} + \nabla \times \frac{1}{\mu_r} \nabla \times \boldsymbol{E} = \frac{\partial \boldsymbol{J}}{\partial t} \quad . \tag{25}$$

Both equations are subject to appropriate boundary conditions, i.e., continuity of tangential field components at material boundaries, Eq.(4), and vanishing tangential electric fields at conductors, Eq.(6).

For both Eq.(24) and Eq.(25), some condition at the far field is also needed if the domain is open [82]. This latter formulation is often preferred, partly because of the self-adjoint operator, natural for the formulation of standard finite element schemes, and partly because of the decoupling between the fields, thus reducing the number of unknowns. However, this formulation also comes with a number of pitfalls as we shall discuss shortly.

Let us first, however, consider schemes for the first order form and introduce the inner product

$$(\boldsymbol{u}, \boldsymbol{v})_\Omega = \int_\Omega \boldsymbol{u} \cdot \boldsymbol{v} \, d\boldsymbol{x} \quad .$$

The variational form of Eq.(3) then follows as

$$\frac{d}{dt}\left(\varepsilon_r \boldsymbol{E}, \boldsymbol{\phi}\right)_\Omega = \left(\nabla \times \boldsymbol{H}, \boldsymbol{\phi}\right)_\Omega + \left(\boldsymbol{J}, \boldsymbol{\phi}\right)_\Omega \quad ,$$

$$\frac{d}{dt}\left(\mu_r \boldsymbol{H}, \boldsymbol{\phi}\right)_\Omega = -\left(\nabla \times \boldsymbol{E}, \boldsymbol{\phi}\right)_\Omega \quad ,$$

$\boldsymbol{\phi}$ is test function, which can be a scalar or a vector valued function. To seek the semi-discrete numerical scheme, assume that the computational domain, Ω, is partitioned into K non-overlapping elements, D, on which the test functions has support.

Let us first consider the simplest case in which the test function is a scalar nodal element, much as is done in classical finite elements [63]. Thus, we assume that the numerical solutions are given as

$$E_h^\alpha(\boldsymbol{x},t) = \sum_i E_i^\alpha(t)\phi_i(\boldsymbol{x}) \quad , \quad H_h^\alpha(\boldsymbol{x},t) = \sum_i H_i^\alpha(t)\phi_i(\boldsymbol{x}) \quad ,$$

where $\alpha = (x,y,z)$, (E_i^α, H_i^α) represents the unknowns, being nodal values or expansion coefficients, and $\phi_i(\boldsymbol{x})$ are the locally defined basis functions which are assumed continuous. Although not generally necessary, in the Galerkin form considered here, the trial and test functions are the same.

Inserting the numerical solutions into the variational statement, yields the semi-discrete form as

$$\begin{aligned}
\mathrm{M}^\varepsilon \frac{d}{dt}\boldsymbol{E}_h^x &= \mathrm{S}^y \boldsymbol{H}_h^z - \mathrm{S}^z \boldsymbol{H}_h^y + \mathrm{M}\boldsymbol{J}_h^x \\
\mathrm{M}^\varepsilon \frac{d}{dt}\boldsymbol{E}_h^y &= \mathrm{S}^z \boldsymbol{H}_h^x - \mathrm{S}^x \boldsymbol{H}_h^z + \mathrm{M}\boldsymbol{J}_h^y \\
\mathrm{M}^\varepsilon \frac{d}{dt}\boldsymbol{E}_h^z &= \mathrm{S}^x \boldsymbol{H}_h^y - \mathrm{S}^y \boldsymbol{H}_h^x + \mathrm{M}\boldsymbol{J}_h^z \\
\mathrm{M}^\mu \frac{d}{dt}\boldsymbol{H}_h^x &= \mathrm{S}^z \boldsymbol{E}_h^y - \mathrm{S}^y \boldsymbol{E}_h^z \\
\mathrm{M}^\mu \frac{d}{dt}\boldsymbol{H}_h^y &= \mathrm{S}^x \boldsymbol{E}_h^z - \mathrm{S}^z \boldsymbol{E}_h^x \\
\mathrm{M}^\mu \frac{d}{dt}\boldsymbol{H}_h^z &= \mathrm{S}^y \boldsymbol{E}_h^x - \mathrm{S}^x \boldsymbol{E}_h^y
\end{aligned} \tag{26}$$

where $(\boldsymbol{E}_h^\alpha, \boldsymbol{H}_h^\alpha)$ represents the global degrees of freedom. We likewise have the globally defined mass matrices

$$\mathrm{M}_{ij}^\varepsilon = \left(\phi_i, \varepsilon_r \phi_j\right)_\Omega \quad , \quad \mathrm{M}_{ij}^\mu = \left(\phi_i, \mu_r \phi_j\right)_\Omega \quad , \mathrm{M}_{ij} = \left(\phi_i, \phi_j\right)_\Omega \quad ,$$

as well as the differentiation matrix

$$\mathrm{S}_{ij}^\alpha = \left(\phi_i, \frac{\partial \phi_j}{\partial \alpha}\right)_\Omega \quad .$$

For the harmonic case, it was shown in [89], however, that this most obvious form harbors spurious vector modes which may lead to convergence to wrong solutions.

This was attributed to a lack of enforcing the constraint of divergence free fields. Another interpretation of this is the inability to properly represent the nulls pace of the curl-operator [115].

This topic of spurious solutions to Maxwell's equations has received significant attention in the literature [89, 98, 65], primarily in the context of frequency domain solutions. An introductory overview is given in [115]. In the time-domain these problems appear to be much less significant and controllable through the smoothness of the initial conditions [65, 72].

Nevertheless, the solutions proposed to overcome problems of spurious modes in frequency domain schemes have generally been used also in the development of schemes for the time-domain. While several solutions are known, the by far most popular is the use of a vectorial basis in the formulation of the finite element schemes, i.e.,

$$\boldsymbol{E}(\boldsymbol{x},t) = \sum_i E_i(t)\boldsymbol{N}_i(\boldsymbol{x}) \quad , \quad \boldsymbol{H}(\boldsymbol{x},t) = \sum_i H_i(t)\boldsymbol{N}_i(\boldsymbol{x}) \quad , \tag{27}$$

where (E_i, H_i) are scalars and $\boldsymbol{N}_i(\boldsymbol{x})$ represents the vectorial basis.

The main motivation for seeking vector basis functions is the observation that the boundary conditions for Maxwell's equations are vectorial, i.e., it is natural when seeking a conforming discretizations to utilize vector basis functions. Such basis functions, often known as curl conforming elements, should satisfy fundamental properties of the solutions to Maxwell's equations, e.g., support tangential continuity of the solutions. This allows for imposing tangential continuity between elements with different materials as well as impose boundary conditions in a natural way. Furthermore, the use of such elements guarantee the absence of spurious modes in frequency-domain finite element schemes [7]. An introduction to vector elements and how they avoid the spurious modes is given in [115].

Such vector elements, known as edge-elements [6], Nedelec elements [93, 94], Whitney forms [6, 56, 57], and curl/div conforming vector elements [40, 2], have a number of interesting properties. In particular, they are constructed to provide a discrete analog to the continuous vector algebra and to enforce only minimal continuity across element boundaries, i.e., the curl conforming elements enforce tangential continuity while the div-conforming elements enforce normal continuity. Albeit at considerable technical effort, edge elements can be constructed to arbitrary high-order, of modal/hierarchic [94, 125, 2] as well as interpolatory type [40], and for simplices as well as quadrilaterals and hexahedrals. A general abstract construction is discussed in [56, 57, 58] and elements suitable for nonuniform order is derived in [22].

Using curl conforming elements, the semi-discrete form of Eq.(24) becomes

$$\mathrm{M}^{\varepsilon}\frac{d}{dt}\boldsymbol{E}_h = \mathrm{S}\boldsymbol{H}_h + \mathrm{M}\boldsymbol{J}_h \quad , \quad \mathrm{M}^{\mu}\frac{d}{dt}\boldsymbol{H}_h = -\mathrm{S}\boldsymbol{E}_h \quad , \tag{28}$$

where $(\boldsymbol{E}_h, \boldsymbol{H}_h)$ again represents the global degrees of freedom. The globally defined mass matrices are given as

$$\mathrm{M}^{\varepsilon}_{ij} = (\boldsymbol{N}_i, \varepsilon_r \boldsymbol{N}_j)_\Omega \quad , \quad \mathrm{M}^{\mu}_{ij} = (\boldsymbol{N}_i, \mu_r \boldsymbol{N}_j)_\Omega \quad , \mathrm{M}_{ij} = (\boldsymbol{N}_i, \boldsymbol{N}_j)_\Omega \quad , \tag{29}$$

as well as the stiffness matrix

$$\mathrm{S}_{ij} = (\boldsymbol{N}_i, \nabla \times \boldsymbol{N}_j)_\Omega \quad .$$

While use of these elements effectively eliminates the spurious modes and adds a lot of structure to the solutions, they do overcome another impact of the conforming finite element scheme, i.e., the need to invert a global, albeit sparse, mass matrix, even if explicit time-stepping is used. As the order of the scheme increases, more degrees of freedom is needed on each element, quickly rendering this inversion prohibitive.

An approach to circumvent this has been developed in [20] where it was demonstrated that one can use mass lumping to diagonalize the mass matrices without sacrificing the accuracy, even on curvilinear elements. This makes the scheme fully explicit at the semi-discrete level and competitive with alternative methods. Unfortunately, this approach is successful only when using quadrilateral and hexahedral Nedelec-type elements as discussed in depth in [20, 19]. The computational results are limited to two dimensional problems. A dispersion analysis of the semi discrete scheme is also included in [20], displaying properties as for the finite difference scheme discussed in Sec. 3.

While the development of the curl-conforming Nedelec elements presents a major advancement, it comes at a slight price. Not only are these families of elements complex but they also have a significantly higher number of degrees of freedom as compared to the classical nodal elements. This is summarized in Table 2, illustrating that the curl-conforming elements typically have d-times more degrees of freedom, d being the dimension of the problem. However, as one needs d scalar fields, the differences are significant for low order elements only.

An alternative to the use of curl-conforming elements, while avoiding to reintroduce the problem of spurious modes, is to change the variation statement to account for the divergence constraint, e.g., as a penalty term

$$\frac{d}{dt}\left(\varepsilon_r \boldsymbol{E}, \boldsymbol{\phi}\right)_\Omega = \left(\nabla \times \boldsymbol{H}, \boldsymbol{\phi}\right)_\Omega + \left(\boldsymbol{J}, \boldsymbol{\phi}\right)_\Omega + \left(\nabla \cdot \varepsilon_r \boldsymbol{E}, \boldsymbol{\phi}\right)_\Omega \quad ,$$

$$\frac{d}{dt}\left(\mu_r \boldsymbol{H}, \boldsymbol{\phi}\right)_\Omega = -\left(\nabla \times \boldsymbol{E}, \boldsymbol{\phi}\right)_\Omega + \left(\nabla \cdot \boldsymbol{H}, \boldsymbol{\phi}\right)_\Omega \quad .$$

Similar forms has been shown to successfully eliminate the spurious modes [65, 64], using the general language of least squares stabilized low order finite element scheme. As promising as this approach appear, we are unaware of any high-order results using this.

While the developments of high-order finite element schemes for the first order system remains limited, there has been more recent activity regarding the development of finite element schemes for Maxwell's equations on the curl-curl form, Eq.(25).

TABLE 2
Degrees of freedom for nodal and curl elements of order n.

	Nodal Element	Curl Element
Quadrilateral	$(n+1)^2$	$2(n+1)(n+2)$
Hexahedral	$(n+1)^3$	$3(n+1)(n+2)^2$
Triangle	$\frac{1}{2}(n+1)(n+2)$	$(n+1)(n+3)$
Tetrahedron	$\frac{1}{6}(n+1)(n+2)(n+3)$	$\frac{1}{2}(n+1)(n+3)(n+4)$

Assuming again the use of scalar nodal finite elements, the strong variational form for Eq.(25) is

$$\frac{d^2}{dt^2}\left(\varepsilon_r \boldsymbol{E}, \phi\right)_\Omega + \left(\nabla \times \frac{1}{\mu_r}\nabla \times \boldsymbol{E}, \phi\right)_\Omega = \frac{d}{dt}\left(\boldsymbol{J}, \phi\right)_\Omega \quad ,$$

resulting in the semi-discrete Galerkin form

$$\begin{aligned}
\mathrm{M}^\varepsilon \frac{d^2}{dt^2}\boldsymbol{E}_h^x + \mathrm{S}^{y,x}\boldsymbol{E}_h^y - \mathrm{S}^{y,y}\boldsymbol{E}_h^x - \mathrm{S}^{z,z}\boldsymbol{E}_h^x + \mathrm{S}^{z,x}\boldsymbol{E}_h^z &= \mathrm{M}\frac{d}{dt}\boldsymbol{J}_h^x \\
\mathrm{M}^\varepsilon \frac{d^2}{dt^2}\boldsymbol{E}_h^y + \mathrm{S}^{z,y}\boldsymbol{E}_h^z - \mathrm{S}^{z,z}\boldsymbol{E}_h^y - \mathrm{S}^{x,x}\boldsymbol{E}_h^y + \mathrm{S}^{x,y}\boldsymbol{E}_h^x &= \mathrm{M}\frac{d}{dt}\boldsymbol{J}_h^y \qquad (30) \\
\mathrm{M}^\varepsilon \frac{d^2}{dt^2}\boldsymbol{E}_h^z + \mathrm{S}^{x,z}\boldsymbol{E}_h^x - \mathrm{S}^{x,x}\boldsymbol{E}_h^z - \mathrm{S}^{y,y}\boldsymbol{E}_h^z + \mathrm{S}^{y,z}\boldsymbol{E}_h^y &= \mathrm{M}\frac{d}{dt}\boldsymbol{J}_h^z
\end{aligned}$$

where

$$\mathrm{S}_{ij}^{\alpha,\beta} = \left(\phi_i, \frac{\partial}{\partial\alpha}\frac{1}{\mu_r}\frac{\partial}{\partial\beta}\phi_j\right)_\Omega \quad ,$$

and the remaining operators are defined as above. It is, however, more common to balance the smoothness between the trial and test functions and consider the weak form

$$\frac{d^2}{dt^2}\left(\varepsilon_r \boldsymbol{E}, \phi\right)_\Omega + \oint_{\partial\Omega}\left(\hat{\boldsymbol{n}} \times \frac{1}{\mu_r}\nabla \times \boldsymbol{E}\right)\phi\, d\boldsymbol{x} - \int_\Omega \nabla\phi \times \frac{1}{\mu_r}\nabla \times \boldsymbol{E}\, d\boldsymbol{x} = \frac{d}{dt}\left(\boldsymbol{J}, \phi\right)_\Omega$$

with a semi-discrete form very similar to that above, Eq. (30).

As for the first order schemes discussed above, much attention has been paid to the problems of spurious modes in the frequency-domain form of the curl-curl equations. Indeed, it was in these schemes that the problems with spurious solutions was first observed [111].

This has lead to several different approaches to overcomes this, following ideas similar to those discussed above. The straightforward approach is to employ high-order curl-conforming elements to eliminate the possibility of spurious modes. Assuming solutions of the form in Eq.(27), this yields the semi-discrete scheme

$$\mathrm{M}^\varepsilon \frac{d^2}{dt^2}\boldsymbol{E}_h - \mathrm{S}\boldsymbol{E}_h = \mathrm{M}\frac{d}{dt}\boldsymbol{J}_h \quad ,$$

where $\boldsymbol{E}_h$ and $\boldsymbol{J}_h$ represents the vectors of global electric fields and currents, the global mass-matrices are defined in Eq.(29), and the stiffness matrix has the entries

$$\mathrm{S}_{ij} = \left(\nabla \times \boldsymbol{N}_i, \frac{1}{\mu_r} \nabla \times \boldsymbol{N}_j \right)_\Omega \quad .$$

As demonstrated recently in [67, 68], this formulation allows for the development of high-order accurate schemes for the time-domain solution of the curl-curl equations. The effort demonstrates the viability of such an approach for solving full three-dimensional time-dependent problems, in combination with perfectly matched layers [66] or a global boundary elements technique [68]. Although the available results remain fairly simple they nevertheless demonstrate the potential of such an approach.

The alternative approach, modifying the variational statement to include the divergence constraint, takes the from [88]

$$\frac{d^2}{dt^2} \left(\varepsilon_r \boldsymbol{E}, \phi \right)_\Omega + \oint_{\partial\Omega} \left(\hat{\boldsymbol{n}} \times \frac{1}{\mu_r} \nabla \times \boldsymbol{E} \right) \phi \, \boldsymbol{x} - \int_\Omega \nabla\phi \times \frac{1}{\mu_r} \times \boldsymbol{E} \, d\boldsymbol{x} + \\ + \int_\Omega \left(\nabla \cdot \varepsilon_r \boldsymbol{E} \right) \nabla\phi \, d\boldsymbol{x} - \oint_{\partial\Omega} \hat{\boldsymbol{n}} \frac{1}{\varepsilon_r \mu_r} \nabla \cdot \varepsilon_r \boldsymbol{E} \phi \, d\boldsymbol{x} = \frac{d}{dt} \left(\boldsymbol{J}, \phi \right)_\Omega \quad .$$

A related approach is discussed in [65, 64], derived using a least squares stabilized finite element scheme, thus avoiding the direct penalization. In [8, 99, 9] it is proposed to solve Maxwell's equations using vector and scalar potentials, likewise eliminating spurious modes. We are unaware of attempts to combine such formulations with high order elements.

7.2. Discontinuous Finite Element Techniques

As promising as the continuous finite element formulation is, it suffers from a number of problems which are not easily overcome. As we have already discussed, the need for a conforming discretization not only complicates matters but also results in the need to invert a global mass matrix at every time step. While this mass matrix is sparse and typically well conditioned the work associated with this inversion increases for higher order methods, becomes significant for large scale problems and may become a bottleneck for parallel computations.

Recently, however, formulations which eliminate these issues has appeared. While they can be derived for Maxwell's equations on both first order form, Eq.(24), as well as for the curl-curl form, Eq.(25), all recent work has focused on the former.

We shall thus seek solution to Eq.(24) in a general domain, Ω considered as the union of non-overlapping body-conforming elements, D. To simplify the derivation we shall furthermore consider Maxwell's equations on conservation form, Eq.(31), as

$$\mathrm{Q}(\boldsymbol{x}) \frac{\partial \boldsymbol{q}}{\partial t} + \nabla \cdot \boldsymbol{F}(\boldsymbol{q}) = \boldsymbol{S}(\boldsymbol{q}^i, \boldsymbol{x}) \quad . \tag{31}$$

Recall that $\boldsymbol{q}$ represents the state vector, the flux $\boldsymbol{F}$ is given in Eq.(23), Q reflects a diagonal matrix with material parameters and $\boldsymbol{S}$ signifies the sources, e.g., the incoming fields and/or the current.

To formulate the scheme we assume that there exists an approximate solution, $\boldsymbol{q}_h$, on the form

$$\boldsymbol{q}_h(\boldsymbol{x},t) = \sum_i \boldsymbol{q}_i(t)\phi_i(\boldsymbol{x}) \ , \tag{32}$$

within each element. Similarly, we assume that $\boldsymbol{F}_h$ and $\boldsymbol{S}_h$ are polynomial representations of the flux and of the source, respectively. Note that we do not place any global constraints on the basis, ϕ_i, i.e., it is in general discontinuous and non-conforming.

To seek equations for the unknowns, we require the approximate solution to Maxwell's equations, $\boldsymbol{q}_h$, to satisfy

$$\begin{aligned}\int_{\mathsf{D}} \Big(\mathrm{Q}\frac{\partial \boldsymbol{q}_h}{\partial t} \ &+ \ \nabla\cdot\boldsymbol{F}_h - \boldsymbol{S}_h)\,\Phi_i(\boldsymbol{x})\,d\boldsymbol{x} \\ &= \oint_{\partial\mathsf{D}} \Psi_i(\boldsymbol{x})\hat{\boldsymbol{n}}\cdot[\boldsymbol{F}_h - \boldsymbol{F}^*]\ d\boldsymbol{x} \ .\end{aligned} \tag{33}$$

We emphasize that the integration is over the local element, D, and not the full domain, Ω, in contrast to the to continuous finite element schemes discussed in Sec. 7.1.

Here Φ_i and Ψ_i represent sequences of N test functions, $\boldsymbol{F}^*$ signifies a numerical flux and $\hat{\boldsymbol{n}}$ is an outward pointing unit vector defined at the boundary of the element. If the numerical flux is consistent, the scheme is clearly consistent. On the other hand, boundary/interface conditions are not imposed exactly but rather weakly through the penalizing surface integral. In this multi-element context, the formulation is inherently discontinuous and yields, through its very construction, a highly parallel local scheme.

Let us define the local inner product

$$(\boldsymbol{u},\boldsymbol{v})_{\mathsf{D}} = \int_{\mathsf{D}} \boldsymbol{u}\cdot\boldsymbol{v}\,d\boldsymbol{x} \ ,$$

and the local mass matrices operators

$$\mathrm{M}^{\varepsilon}_{ij} = (\Phi_i,\varepsilon_r\phi_j)_{\mathsf{D}} \ , \ \mathrm{M}^{\mu}_{ij} = (\Phi_i,\mu_r\phi_j)_{\mathsf{D}} \ , \ \mathrm{M}_{ij} = (\Phi_i,\phi_j)_{\mathsf{D}} \ , \tag{34}$$

the discrete differentiation operator

$$\mathrm{S}^{\alpha}_{ij} = \left(\Phi_i, \frac{\partial}{\partial\alpha}\phi_j\right)_{\mathsf{D}} \ , \tag{35}$$

where $\alpha = (x,y,z)$. The boundary integration operator is defined as

$$\mathrm{F}_{ij} = \oint_{\partial\mathsf{D}} \Psi_i\phi_j\,d\boldsymbol{x} \ . \tag{36}$$

With this, we can write the semi-discrete form of Maxwell's equations as

$$
\begin{aligned}
&\mathrm{M}^{\varepsilon}\frac{d}{dt}\boldsymbol{E}_h^x - \mathrm{S}^y\boldsymbol{H}_h^z + \mathrm{S}^z\boldsymbol{H}_h^y - \mathrm{M}\boldsymbol{S}_h^{E,x} = \mathrm{F}\boldsymbol{P}_h^{E,x} \\
&\mathrm{M}^{\varepsilon}\frac{d}{dt}\boldsymbol{E}_h^y - \mathrm{S}^z\boldsymbol{H}_h^x + \mathrm{S}^x\boldsymbol{H}_h^z - \mathrm{M}\boldsymbol{S}_h^{E,y} = \mathrm{F}\boldsymbol{P}_h^{E,y} \\
&\mathrm{M}^{\varepsilon}\frac{d}{dt}\boldsymbol{E}_h^z - \mathrm{S}^x\boldsymbol{H}_h^y + \mathrm{S}^y\boldsymbol{H}_h^x - \mathrm{M}\boldsymbol{S}_h^{E,z} = \mathrm{F}\boldsymbol{P}_h^{E,z} \\
&\mathrm{M}^{\mu}\frac{d}{dt}\boldsymbol{H}_h^x - \mathrm{S}^z\boldsymbol{E}_h^y + \mathrm{S}^y\boldsymbol{E}_h^z - \mathrm{M}\boldsymbol{S}_h^{H,x} = \mathrm{F}\boldsymbol{P}_h^{H,x} \\
&\mathrm{M}^{\mu}\frac{d}{dt}\boldsymbol{H}_h^y - \mathrm{S}^x\boldsymbol{E}_h^z + \mathrm{S}^z\boldsymbol{E}_h^x - \mathrm{M}\boldsymbol{S}_h^{H,y} = \mathrm{F}\boldsymbol{P}_h^{H,y} \\
&\mathrm{M}^{\mu}\frac{d}{dt}\boldsymbol{H}_h^z - \mathrm{S}^y\boldsymbol{E}_h^x + \mathrm{S}^x\boldsymbol{E}_h^y - \mathrm{M}\boldsymbol{S}_h^{H,z} = \mathrm{F}\boldsymbol{P}_h^{H,z} \quad .
\end{aligned} \tag{37}
$$

Here $(\boldsymbol{E}_h^{\alpha}, \boldsymbol{H}_h^{\alpha})$, $\alpha = (x, y, z)$, represents the local degrees of freedom, $\boldsymbol{S}^{E,\alpha}$ and $\boldsymbol{S}^{H,\alpha}$ represents the components of the sources discussed in Sec. 2, and we have introduced the penalizing boundary fluxes, $\boldsymbol{P}_h^{E,\alpha}$ and $\boldsymbol{P}_h^{H,\alpha}$ for $\boldsymbol{E}_h$ and $\boldsymbol{H}_h$, respectively. We shall define these shortly.

One notes immediately that relaxing the continuity of the elements decouples the elements and results in a block-diagonal global mass matrix which can be inverted in preprocessing. The price paid for this is the additional degrees of freedom needed to support the local basis functions. For high-order elements, this is, however, only a small fraction of the total number of degrees of freedom.

The coupling of the local solutions to recover the global solution is accomplished through the numerical fluxes, $\boldsymbol{F}^*$. In this regard, one can view these methods as a high-order generalization of the finite volume schemes discussed in Sec. 6, albeit without the complications of wide stencils and complex procedures for the reconstruction of the pointwise solution.

Given the linearity of Maxwell's equations, it is natural to use upwinding, similar to the patching through characteristics discussed for the spectral multidomain schemes in Sec. 5. This is given on the form [90]

$$
\boldsymbol{P}_h^E = \overline{Z}^{-1}\hat{\boldsymbol{n}} \times \left(\hat{\boldsymbol{n}} \times [\boldsymbol{E}_h] - Z^+[\boldsymbol{H}_h]\right) \quad , \tag{38}
$$

$$
\boldsymbol{P}_h^H = \overline{Y}^{-1}\hat{\boldsymbol{n}} \times \left(\hat{\boldsymbol{n}} \times [\boldsymbol{H}_h] + Y^+[\boldsymbol{E}_h]\right) \quad . \tag{39}
$$

Here $[\boldsymbol{q}] = \boldsymbol{q}^- - \boldsymbol{q}^+$ measures the jump in the field values across an interface. Superscript '+' refers to field values from the neighbor element while superscript '-' refers to field values local to the element. To account for the potential differences in material properties in the two elements, the local impedance, $Z^{\pm}$, and conductance, $Y^{\pm}$, is defined as

$$
Z^{\pm} = \frac{1}{Y^{\pm}} = \sqrt{\frac{\mu^{\pm}}{\varepsilon^{\pm}}} \quad ,
$$

and the sums

$$\overline{Z} = Z^+ + Z^- \ , \ \overline{Y} = Y^+ + Y^- \ ,$$

of the local impedance and conductance, respectively.

Choosing the test functions, Φ_i, Ψ_i and the numerical flux, $\boldsymbol{F}^*$, one has a large degree of freedom when designing different schemes. Focusing on Galerkin schemes, in which case $\Psi_i(\boldsymbol{x}) = \Phi_i(\boldsymbol{x}) = \phi_i(\boldsymbol{x})$, it is worth realizing that following integration by parts in Eq.(33) this scheme becomes the much studied discontinuous Galerkin method [18, 3]. This is, however, only one among many different formulations in the same family of discontinuous element/Penalty methods. We refer to [50, 52, 53] where other choices are studied in the general context of conservation laws and problems of wave-propagation.

To complete the scheme one needs to specify basis element type and an associated basis $\phi_i(\boldsymbol{x})$, most often of polynomial nature. and define the unknown coefficients, $\boldsymbol{q}_h$, for functions defined on the elements.

Using general curvilinear quadrilaterals, as in [78, 79], it is natural to use a tensor-product interpolating basis as is done for the spectral multi-domain schemes discussed in Sec. 5.2. The advantage of this is, apart from its simplicity, that one recovers a diagonal local mass matrix by using polynomials defined at quadrature points. This results in schemes that are very similar to those in Sec. 5.2, the main difference being whether the characteristic conditions on the boundary fluxes are imposed weakly or strongly. A non-conforming extension of such schemes is discussed in [79] and the dispersion characteristics of such schemes are discussed in [61]. Extensions to problems with nonuniform grids are analyzed in [62], confirming that such discontinuous formulations are well suited for wave-propagation.

In [123, 54, 55] the development of a Galerkin scheme on nodal tetrahedral elements is initiated, aimed at demonstrating the potential of using a discontinuous element formulation for solving very large geometrically complex three-dimensional problems in time-domain computational electromagnetics.

Choosing the appropriate form of the local basis on the tetrahedron is less a question of formulation and more a question of performance as measured by efficiency and accuracy of the final scheme. An immediate candidate is the monomial basis, $\phi_i(\boldsymbol{x}) = x^{\alpha_1} y^{\alpha_2} z^{\alpha_3}$ with $|\boldsymbol{\alpha}| \leq n$. As is well known, however, this will lead to extremely illconditioned operators as the basis becomes almost linearly dependent for high polynomial order and prohibits the stable and accurate computation at high order.

The way to overcome such conditioning problems, we first follow the approach of Sec. 5.2, and introduce a smooth curvilinear mapping, $\Psi : \mathsf{D} \rightarrow \mathsf{I}$, between the general element, D, and a canonical tetrahedron, I, on which we seek an orthonormal basis. Such a basis has been known for a long time [103, 75, 27]. This leaves the question of how to compute the expansion coefficients, $\boldsymbol{q}$. Clearly, with an orthonormal basis at hand, it may seem natural to use this as the local basis. The impact of doing so, however, is that all modes are needed to evaluate $\boldsymbol{q}_h$ pointwise. This lack of separation between inner modes and boundary modes is not optimal for the discontinuous formulation where the flux term depends on the fluxes at the boundary of D only. To overcome this issue one could seek to give up the strict

orthonormality of the basis to achieve a separation between inner and boundary modes. Such a basis is developed in [73] and provides an approach, albeit rather complex, to achieve arbitrarily high order accuracy.

Using a nodal element, however, one can define $\boldsymbol{q}_h$ as an interpolating polynomial, i.e., we require that

$$\forall i \ : \ \boldsymbol{q}_h(\boldsymbol{x}(\boldsymbol{\xi}_i),t) = \sum_j \boldsymbol{q}_j(t)\phi_j(\boldsymbol{\xi}_i) \ ,$$

where $\phi_j(\boldsymbol{\xi})$ is the orthonormal basis on I and $\boldsymbol{\xi}_i$ are predefined grid-points in I. The number of nodes, N, is simply that required for completeness, as listed in Table 2. On vector form this yields the requirement that

$$\boldsymbol{q}_h = \mathrm{V}\boldsymbol{q} \ , \ \ \mathrm{V}_{ij} = \phi_j(\boldsymbol{\xi}_i) \ , \tag{40}$$

where V is a multidimensional Vandermonde matrix. The genuine multivariate Lagrangian polynomials are

$$\boldsymbol{q}_h(\boldsymbol{x}(\boldsymbol{\xi}),t) = \sum_{i=1}^{N} \boldsymbol{q}_h(\boldsymbol{x}(\boldsymbol{\xi}_i),t)L_i(\boldsymbol{\xi}) \ , \ \ \mathrm{V}^T\boldsymbol{L} = \boldsymbol{\phi} \ ,$$

where the latter expression for evaluation of the Lagrange polynomials follows from the interpolation property. Here $\boldsymbol{L} = [L_1(\boldsymbol{\xi}),..,L_N(\boldsymbol{\xi})]^T$ and the basis is given as $\boldsymbol{\psi} = [\phi_1(\boldsymbol{\xi}),..,\phi_N(\boldsymbol{\xi})]^T$.

The final issue in need of attention is the choice of the nodal points, $\boldsymbol{\xi}_i$, within I. As is well known, the success of high-order Lagrangian interpolation is critically dependent on the correct distribution of the nodes. This is a problem that has received some attention recently and nodal distributions, enabling the construction of well behaved unique Lagrange polynomials up to order 18 on the triangle [49] and up to order 10 on the tetrahedron [16, 53].

The nodal distributions are characterized by having exactly N nodes. Furthermore, the nodal set includes the vertices, the edges, and the faces of the tetrahedron. The number of nodes on each face is exactly that is required to support a two-dimensional multivariate polynomial, i.e., $N_{2d} = (n+1)(n+2)/2$ nodes on each face. Same characteristics are shared by the nodes on the triangles.

In this setting it is more natural to recast the scheme in physical space. The only difference with Eq.(37) is that $(\boldsymbol{E}_h^\alpha, \boldsymbol{H}_h^\alpha)$ then represents the N-long vectors of nodal values in each element, $\boldsymbol{S}_h$ the nodal values of the source function, and $\boldsymbol{P}_h^E$ and $\boldsymbol{P}_h^H$ the nodal values of the numerical flux as defined in Eqs.(38)-(39).

The discrete, pointwise operators, are given as

$$\mathrm{M}_{ij} = \int_{\mathsf{D}} L_i L_j \, d\boldsymbol{x} \ , \ \ \mathrm{S}_{ij}^\alpha = \int_{\mathsf{D}} L_i \frac{\partial L_j}{\partial \alpha} \, d\boldsymbol{x} \ . \tag{41}$$

The form of the boundary operator, F, is simplified as a consequence of the uniqueness of the Lagrange polynomial and the structure of the nodal points, i.e., integration of the three-dimensional L_i over the surface is equivalent to the sum of

the integration of the two-dimensional Lagrange polynomials defined by the nodal distribution on the faces. This implies that

$$\begin{aligned} \mathrm{F}_{ij}^{\mathrm{face}} &= \oint_{\mathrm{face}} l_i^{2D} l_j^{2D} d\boldsymbol{x} \quad , \\ \mathrm{F} &= \sum_{\mathrm{faces}} \mathrm{R}_{face}^T (\mathrm{V}_{2D}^{-1})^T \mathrm{F}^{\mathrm{face}} \mathrm{V}_{2D}^{-1} \mathrm{R}_{face} \quad . \end{aligned} \tag{42}$$

Here l_i^{2D} represents the two-dimensional Lagrange polynomials defined by the nodes on each of the 4 faces, V_{2D} is the associated Vandermonde matrix similar to the three-dimensional form, Eq.(40), and R_{face} is an $N_{2d} \times N$ which serves to extract those nodes situated at each face of the element.

To reiterate the importance of this separation between internal and boundary nodes, we note that the operation count for evaluating the scheme, Eq.(37), assuming no separation, is $\mathcal{O}(6N^2)$ for each variable. For the nodal scheme, or a modal scheme with a similar separation, the work scales like $\mathcal{O}(2N^2 + 4NN_{2d})$. Hence, the relative saving in operations scales as

$$\frac{\text{Work with Nodal Basis}}{\text{Work with Simple Modal Basis}} = \frac{1}{3} + \frac{2}{n+3} \quad .$$

This clearly becomes increasingly important as the order of the approximation, n, increases, although even for $n = 3$ do we find a $1/3$ reduction.

One of the main advantages of the nodal element is the ease by which one can relax the restriction on tetrahedra having straight faces only. Clearly, this will impact the evaluation of the discrete operators, Eqs.(41)-(42), by requiring specific operators for each element and sufficient accuracy in the integration to evaluate entries in the operators. However, the evaluation of the boundary fluxes is straightforward in a nodal representation even as the normal vectors, $\hat{\boldsymbol{n}}$, vary along the faces.

The details of the nodal based discontinuous element scheme and its efficient implementation can be found in [54, 55], including a complete convergence analysis and alternative divergence preserving formulations.

The discontinuous element formulation can be expected discussed to allow a highly efficient parallel implementation on contemporary large scale distributed memory machines. As a verification of this, we list in Table 3 the relative parallel speedup for a single large scale application, demonstrating superlinear scaling. Similar and more extensive studies, given in [54], confirm this high parallel efficiency for a variety of applications.

TABLE 3
Relative time for a 245.000 element grid with 6'th order elements as a function of the number of processors.

Number of Processors	64	128	256	512
Relative time	1.00	0.48	0.24	0.14

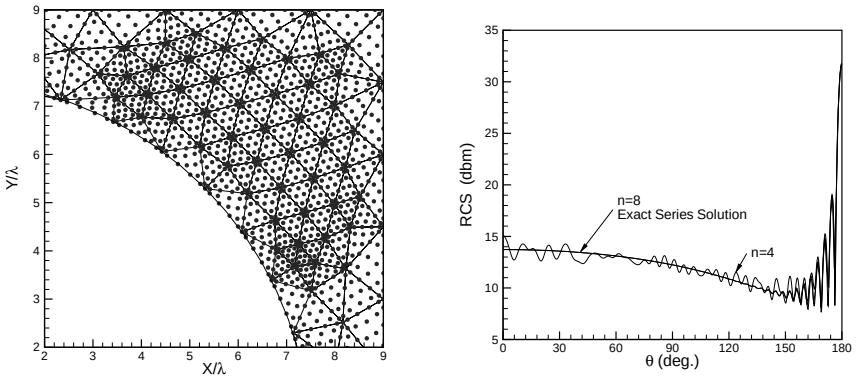

FIG. 14. On the left is shown details of the body conforming grid used to compute scattering by a two-dimensional PEC cylinder. The right shows the rapidly converging bistatic radar-cross-section when increasing the order, n, of the scheme.

Let us conclude this discussion with a few examples. Advancement in time is done using a low-storage 4th order explicit Runge-Kutta method [14] and the computational domain is terminated with a combination of stretching of the grid and characteristic boundary conditions at the outer boundaries.

As a first, simple two-dimensional problem, we consider TM-polarized plane wave scattering by a $ka = 15\pi$ metallic cylinder . In Fig. 14 we show both a fraction of the grid, illustrating the body conforming high-order nodal grid, and the bistatic RCS computed using a fixed, very coarse grid, and achieving convergence by increasing the order of the scheme.

As an example of a more challenging three-dimensional problem, consider plane wave scattering by a perfectly conducting conesphere, consisting of a 60.5 cm long cone with half angle of 7 deg, capped smoothly with a spherical cap of radius 7.49

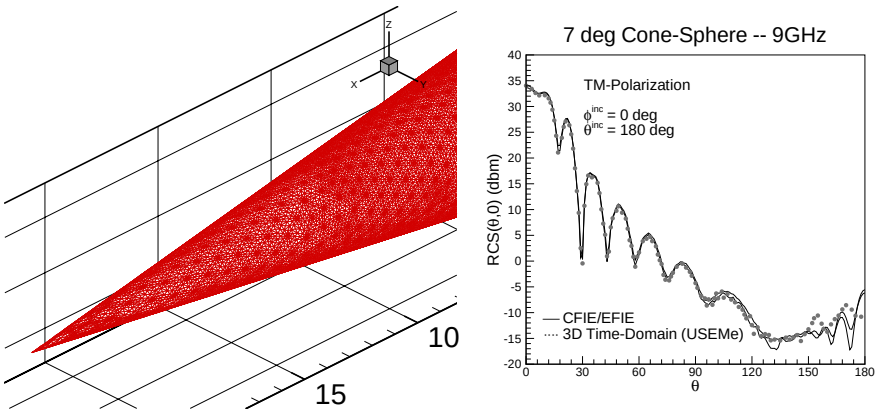

FIG. 15. On the left we show a details of the body conforming grid used to compute scattering by a large PEC conesphere. The surfaces are triangulated for visualization based on the nodes of the high-order elements. On the right we show computed bistatic radar-cross-section (RCS) for vertically polarized plane wave illumination at the tip and compared with results using integral equation based frequency domain solver (CFIE).

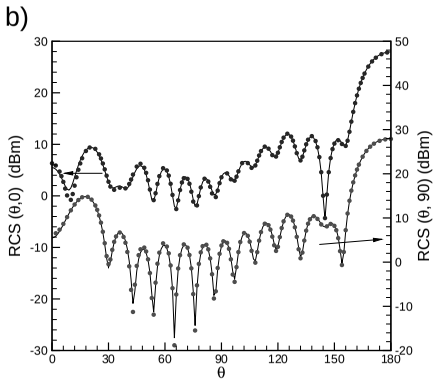

FIG. 16. Scattering by a finite length di-electric cylinder with $\varepsilon_r = 2.25$. We show the RCS(θ,0) for vertical polarization ($\cdot$) of the illuminating field and RCS(θ,90) for horizontal polarization ($\cdot$) compared with results obtained using a spectral multi-domain axi-symmetric code (full line) [130]

cm. Illuminated by a 9 GHz plane wave, the object is approximately 21 wavelengths long. What makes the problem challenging, though, is not only its electric size but also the very sharp apex and the long shadow region.

In Fig. 15 we show a detail of the grid near the apex as well as the full bistatic cross-section for axial plane wave illumination of the conesphere, showing excellent agreement with high fidelity results obtained using a CFIE integral equation solver. The computation utilizes about 270.000 tetrahedral elements at 3rd order with a resolution at the surface of up to 20 points/wavelength. We note the excellent agreement and a dynamic range exceeding 50 db. Similar results and agreement have been found for TE polarized illumination.

As an example of a problem, involving penetration, we consider plane wave scattering by a dielectric cylinder, 5λ long, radius of 1 λ and made of a non-magnetic material with a permittivity of $\varepsilon_r = 2.25$, similar to that of glass. We find that using approximately 67.000 elements, supporting a 4th order approximation and with an average vacuum edge length at the cylinder of $\lambda/3$, suffices to accurately predict the far field scattering.

As a final example, illustrating the level of complexity that can currently be considered with this formulation, we show in Fig. 17 a part of a 245.000 element grid for 600 MHz scattering by a military aircraft. Shown is also one of the field components on the surface of the aircraft.

Many more example of the geometric flexibility and high-order accuracy of this approach for the time-domain solution of Maxwell's equations can be found in [54, 55], including scattering by aircraft configurations in the GHz regime.

8. ISSUES IN TEMPORAL INTEGRATION

The discussion of the various schemes has so far focused on the spatial discretization of Maxwell's equations, leading to systems of ordinary differential equations. To solve these, a number of techniques are available in the literature, and the majority of high-order spatial discretization schemes is combined with standard

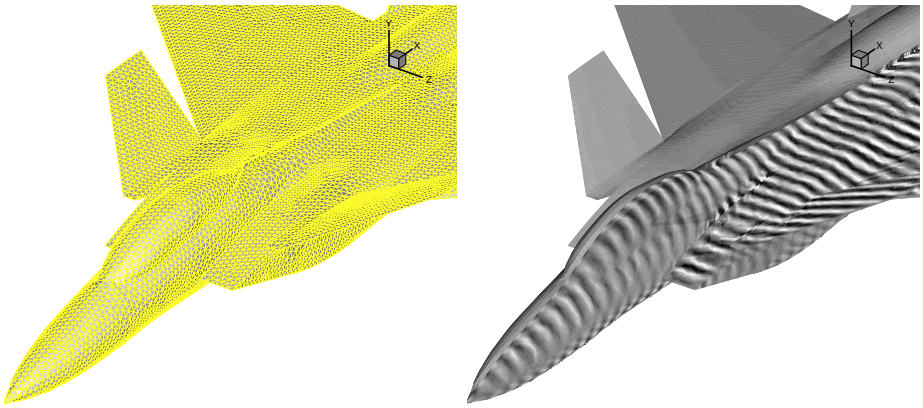

FIG. 17. Application of an unstructured grid discontinuous element high-order method to the solution of electromagnetic scattering a military aircraft. The frequency of the incoming plane wave is 600 MHz. On the left is shown a part of the triangulated surface grid and on the right is shown one of the magnetic field components on the surface of the plane. The computation is performed with 4th order elements and approximately 245.000 tetrahedra to fill the computational volume.

methods such as explicit 3rd or 4th order Runge-Kutta methods [10, 46]. Interesting alternatives to these classical approaches are low-storage Runge-Kutta methods [10, 14], limiting the need for additional stages, and dispersion optimized Runge-Kutta schemes [60], designed for propagating waves over long distances.

Using a spatial high-order finite difference scheme, many practitioners continue to use the 2nd order accurate Leapfrog scheme, used also in the classical Yee scheme [132], often choosing the time-step under error constraints rather than stability constraints. This approach is used in e.g. [119, 135, 134]. In [126] a deferred correction technique using a backward differentiation method is used to achieve 4th order.

The situation is very similar when using finite volume or finite element discretizations of the first order Maxwell's equations where 2nd order Leapfrog schemes [20, 19] or explicit Runge-Kutta methods [33, 34, 35] remain the main workhorses. For the finite element discretizations of the curl-curl equations, leading to an equation of 2nd order in time, the standard choice is the Newmark scheme [63], generally chosen to be 2nd order accurate and either implicit or explicit [66, 68]. Interesting alternatives could be Nyström methods to enable a higher order accuracy. As the finite element discretization of the curl-curl form always requires a matrix inversion, implicit schemes seems most attractive as they come at little additional cost.

The conditions for discrete stability naturally depends on both the details of the spatial and the temporal discretization as well as the form in which Maxwell's equations are stated. However, combining any of the semi-discrete schemes discussed here with an explicit time-integration scheme generally yields a condition for discrete stability as

$$\Delta t \leq C \min_{\Omega} \sqrt{\varepsilon_r \mu_r} h \quad .$$

What separates the different schemes is partly the value of the constant C, typically of $\mathcal{O}(1)$, but most importantly what the grid size, h, means. Naturally, for the extensions of the Yee scheme discussed in Sec. 4 or the high-order finite volume schemes in Sec. 5, h maintains its simple meaning due to the equidistant grid. However, for the more complicated multi-domain/multi-element schemes, the geometric flexibility comes at a price since typically one has

$$h \propto \frac{l}{n^2} \ ,$$

where n represents the order of the approximation and l the smallest edge length of the elements. This illustrates that one should strive to use a large elements as possible to avoid prohibitively small time-steps and, thus, very long computing times. Some attempts to slightly improve on this are discussed in [25, 31, 51] although one has to be careful not to increase the time-step at the expense of accuracy. Ultimately, this emphasizes the need to support curvilinear body-conforming elements in the formulation as one must aim to resolve the solutions and not the geometry since the latter may result in unnecessarily small stable time steps.

As applications become increasingly complex, the geometries themselves often requires small cells and, thus, small time steps. Techniques to overcome this remain active research areas. Fully implicit time-stepping is of course an option but may be prohibitive for large scale problems where the stiffness is localized to small regions of the grid. More interesting alternatives include the use of non-conforming discretizations [22, 79], explicit-implicit Runge-Kutta methods [74] enabling splitting on the grid, and time-accurate local time-stepping methods [21].

9. CONCLUSIONS AND OUTLOOK

Looking through the list of references accompanying this review, one quickly realizes that most references directly related to the high-order accurate time-domain solution of Maxwell's equation are less that 5 years old. This is both a testament to the timeliness of this review as well as the activity experienced in this research area over the last few years.

However, learning about the various efforts also emphasizes that much work remains to be done. The simplicity of the finite difference bases embedding schemes, avoiding grid generation and allowing the treatment of complex, even moving, boundaries in a simple manner, is also its Achilles Heel, i.e., it is difficult to imagine higher than 4th order accuracy and many issues related to stability of general interfaces remains open. However, 4th order may well suffice for many problems of moderate size and complexity. Indeed, if stable and robust versions of such methods could be developed, they may well have the potential to succeed the current golden standard – the Yee scheme.

Currently, however, there seems to be no robust alternative to multi-element schemes, be they spectral multi-domain schemes, high-order time-domain finite element schemes, or discontinuous finite element schemes. Each of these formulations have their own advantages and disadvantages although, at this particular point in time, the development of the discontinuous element formulations, Sec. 7.2, appear to be most advanced.

Many issues continue to require serious attention. Apart from the plentiful theoretical questions, e.g., semi-discrete and fully discrete stability, smoothness of the solutions around non smooth geometries and its impact on the convergence rate, the importance of the divergence constraints in time-domain schemes etc, many issues with a potential for immediate impact remains open. Perhaps most evident is the need to consider alternatives to the widely used explicit time-stepping schemes. For large scale geometrically complex problems this is becoming a bottleneck.

Another area that continues to require attention is the development of accurate and efficient means to truncate the computational domain. This becomes of increasing importance as the accuracy requirements increase. Perfectly matched layer methods [4, 5] have received much attention in the last decade and continues to be a viable solution. Their cost for large scale problems is, however, a concern. Global boundary conditions, e.g., [45, 42, 105], deserves serious attention as does the recently demonstrated use of time-domain integral equations [68] as a means to truncate the computational domain when using high-order accurate methods.

High-order accurate multi-element techniques are currently limited by low-order grid generation, i.e., most commercial grid-generation software does not support higher order descriptions of boundaries and interfaces. To fully ripe the benefits of the high-order accuracy, this must be overcome, e.g., through a more dynamic interface between the model description and the grid generation. This problem is, however, not unique to electromagnetics and there is currently significant research activity to overcome this restriction and enable high-order model description and grid-generation.

Adaptive solution techniques as well as accurate and efficient means to treat randomness in the geometries, materials, and solutions, are both areas which have received only very limited attention in the past. Nevertheless, advances in these areas have the potential for a dramatic impact as applications continues to emphasise higher frequencies and more complex signals form and materials.

While it took the insight of Maxwell to realize the beautiful simplicity of electromagnetic wave propagation, the recent advances in high-order accurate methods for such phenomena suggests that less can do when it comes to solving them computationally. As complex as these problems are, the advances over the last decade are substantial and encouraging, although the applications continue to surpass the computational capabilities in complexity and size. Nevertheless, the gap is slowly narrowing, and the continued emphasis on high-order accurate methods for the time-domain solution of Maxwell's equations may eventually enable the development of robust, accurate, and efficient computational tools, powerful and versatile enough to address the electromagnetic problems of tomorrow.

ACKNOWLEDGMENT

Much of the work contained here was done in collaboration with many collaborators through an extended period of time. Special thanks goes to Cedric Chauviere, Adi Ditkowski, Palle Dinesen, David Gottlieb, Jiaming Jin, Eli Turkel, Tim Warburton, Daniel White, and Baolin Yang for comments, suggestions, and fruitful collaborations over the years. Thanks also to Bengt Fornberg and Tobin Driscoll for providing graphical material.

This work was partly supported by NSF under contract DMS-0074257, ARO under contract DAAD19-01-1-0631, by AFOSR/DARPA under contract F49620-1-0426, and by the Alfred P. Sloan Foundation through a Sloan Research Fellowship.

REFERENCES

1. S. Abarbanel, A. Ditkowski, and A. Yefet, *Bounded Error Schemes for the Wave Equation on Complex Domains* – submitted.
2. M. Ainsworth and J. Coyle, *Hierarchic Finite Element Bases on Unstructured Tetrahedral Meshes*, 2002 – submitted.
3. H. Atkins and C.W. Shu, *Quadrature-Free Implementation of Discontinuous Galerkin Methods for Hyperbolic Equations*, AIAA J. **36**(1998), pp. 775-782.
4. J. P. Berenger, *A Perfectly Matched Layer for the Absorption of Electromagnetic Waves*, J. Comput. Phys. **114**(1994), pp. 185-200.
5. J. P. Berenger, *Three-Dimensional Perfectly Matched Layer for the Absorption of Electromagnetic Waves*, J. Comput. Phys. **127**(1994), pp. 363-379.
6. A. Bossavit, *A Rationale for "Edge-Elements" in 3-D Fields Computations*, IEEE Trans. Magnetics **24**(1988), pp. 74-79.
7. A. Bossavit, *Solving Maxwell's Equations in a Closed Cavity, and the Question of Spurious Modes*, IEEE Trans. Mag. **26**(1990), pp. 702-705.
8. W. E. Boyse, D. R. Lynch, K. D. Paulsen, and G. N. Minerbo, *Nodal-Based Finite Element Modeling of Maxwell's Equations*, IEEE Trans. Antennas Propagat. **40**(1992), pp. 642-651.
9. W. E. Boyse and K. D. Paulsen, *Accurate Solutions of Maxwell's Equations Around PEC Corners and Highly Curved Surfaces Using Nodal Finite Elements*, IEEE Trans. Antennas Propagat. **45**(1997), pp. 1758-1767.
10. J. C. Butcher, *The Numerical Analysis of Ordinary Differential Equations. Runge-Kutta and General Linear Methods*, John Wiley & Sons, New York, 1987.
11. C. Canuto, M. Y. Hussaini, A. Quarteroni, and T. A. Zang, *Spectral Methods in Fluid Mechanics*, Springer Verlag, New York, 1988.
12. M. H. Carpenter, D. Gottlieb, and S. Abarbanel, *Stable and Accurate Boundary Treatments for Compact, High-Order Finite-Difference Schemes*, Appl. Numer. Math. **12**(1993), pp. 55-87.
13. M. H. Carpenter, D. Gottlieb, and S. Abarbanel, *Time-Stable Boundary Conditions for Finite-Difference Schemes Solving Hyperbolic Systems: Methodology and Applications to High-Order Compact Schemes*, J. Comput. Phys. **111**(1994), pp. 220-236.
14. M. H. Carpenter and C. A. Kennedy, *Fourth order 2N-storage Runge-Kutta scheme*, NASA-TM-109112, NASA Langley Research Center, VA. 1994.
15. Z. J. Cendes and P. Silvester, *Numerical Solution of Dielectric Loaded Waveguides. I - Finite Element Analysis*, IEEE Trans. Microwave Theo. Tech. **18**(1971), pp. 1124-1131.
16. Q. Chen and I. Babuška, *The Optimal Symmetrical Points for Polynomial Interpolation of Real Functions in a Tetrahedron*, Comput. Methods Appl. Mech. Engrg. **137**(1996), pp. 89-94.
17. W. C. Chew, J. Jin, E. Michielssen, and J. Song (Eds.), *Fast and Efficient Algorithms in Computational Electromagnetics*, Artech House, Bosotn, 2001.
18. B. Cockburn and C.W. Shu, *Runge-Kutta Discontinuous Galerkin Methods for Convection-Dominated Problems*, J. Sci. Comput. **16**(2001), pp. 173-261.
19. G. C. Cohen, *Higher-Order Numerical Methods for Transient Wave Equations*. Springer-Verlag, Berlin, 2002.
20. G. Cohen and P. Monk, *Mur-Nedelec Finite Element Schemes for Maxwell's Equations*, Comput. Methods Appl. Mech. Engrg. **169**(1999), pp. 197-217.
21. C. Dawson and R. Kirby, *High Resolution Schemes for Conservation Laws with Locally Varying Time Steps*, SIAM J. Sci. Comput. **22**(2001), pp. 2256-2281.
22. L. Demkowicz and L. Vardapetyan, *Modeling of Electromagnetic Absorption/Scattering using hp-adaptive Finite Elements*, Comput. Methods Appl. Mech. Engrg. **152**(1998), pp. 103-124.

23. P. G. Dinesen, J. S. Hesthaven, and J. P. Lynov, 2000, *Rigorous Analysis of Focusing Grating Couplers Using a Time-Domain Spectral Collocation Method.* In Diffractive/Holographic Technologies and Spatial Light Modulators 7. Optoelectronics 2000, San Jose, CA. Cindrich, I.; Lee, S.H.; Sutherland, R.L. (eds.), (International Society for Optical Engineering, Bellingham, WA, 2000), Proceedings of SPIE **3951**, 11-19.

24. A. Ditkowski, K. Dridi, and J. S. Hesthaven, *Convergent Cartesian Grid Methods for Maxwell's Equations in Complex Geometries*, J. Comput. Phys. **170**(2001), pp. 39-80.

25. T. A. Driscoll and B. Fornberg, *A Block Pseudospectral Method for Maxwell's Equations: I. One-Dimensional Case*, J. Comput. Phys. **140**(1998), pp. 47-65.

26. T. A. Driscoll and B. Fornberg, *Block Pseudospectral Methods for Maxwell's Equations: II. Two-dimensional, Discontinuous-Coefficient Case*, SIAM J. Sci. Comput. **21**(1999), pp. 1146-1167.

27. M. Dubiner, *Spectral Methods on Triangles and Other Domains*, J. Sci. Comput. **6**(1991), pp. 345-390.

28. G. X. Fan, Q. H. Liu, and J. S. Hesthaven, *Multi-Domain Pseudospectral Time-Domain Simulations of Scattering by Objects Buried in Lossy Media*, IEEE Trans. Geosci. Remote Sens. **40**(2002), pp. 1366-1373.

29. J. Fang, *Time-Domain Finite-Difference Computation for Maxwell's Equations.* PhD-thesis, UC Berkeley, 1989.

30. P. Fischer and D. Gottlieb, *On the Optimal Number of Subdomains for Hyperbolic Problems on Parallel Computers*, Int. J. Supercomputer Appl. High Perfrom. Comput. **11**(1997), pp. 65-76.

31. B. Fornberg, *A Practical Guide to Pseudospectral Methods.* Cambridge University Press, Cambridge, UK. 1996.

32. B. Fornberg, *Calculation of Weights in Finite Difference Formulas*, SIAM Rev **40**(1998), pp. 685-691.

33. D. Gaitonde and J. S. Shang, *High-Order Finite-Volume Schemes in Wave Propagation Phenomena*, AIAA Paper 96-2335, 34th Aerospace Sciences Meeting & Exhibit, Reno, NV, 1996.

34. D. Gaitonde and J. S. Shang, *Optimized Compact-Difference-Based Finite Volume Schemes for Linear Wave Phenomena*, J. Comput. Phys. **138**(1997), pp. 617-643.

35. D. Gaitonde, J. S. Shang, J. L. Young, *Practical Aspects of High-Order Accurate Finite-Volume Schemes for Electromagnetics*, AIAA Paper 97-0363, 35th Aerospace Sciences Meeting & Exhibit, Reno, NV, 1997.

36. S. V. Georgakopoulos, C. R. Birtcher, C. A. Balanis, and R. A. Renaut, *Higher-Order Finite-Difference Schemes for Electromagnetic Radiation, Scattering, and Penetration, Part I: Theory*, IEEE Antennas Propagat. Mag. **44**(2002), pp. 134-142.

37. S. V. Georgakopoulos, C. R. Birtcher, C. A. Balanis, and R. A. Renaut, *Higher-Order Finite-Difference Schemes for Electromagnetic Radiation, Scattering, and Penetration, Part 2: Applications*, IEEE Antennas Propagat. Mag. **44**(2002), pp. 92-101.

38. W. J. Gordon and C. A. Hall, *Transfinite element methods: Blending-Function Interpolation over Arbitrary Curved Element Domains*, Numer. Math. **21**(1973), pp. 109–129.

39. D. Gottlieb and J. S. Hesthaven, *Spectral Methods for Hyperbolic Problems*, J. Comp. Appl. Math. **128**(2001), pp. 83-131.

40. R. D. Graglia, D. R. Wilton, and A. F. Peterson, *Higher Order Interpolatory Vector Bases for Computational Electromagnetics*, IEEE Trans. Antennas Propagat. **45**(1997), pp. 329-342.

41. R. D. Graglia, R. J. Lubbers, and D. R. Wilton (Eds), *Special Issue on Advanced Numerical Techniques in Electromagnetics*, IEEE Trans. Antennas Propagat. **45**(1997).

42. M. J. Grote and J. B. Keller, *Non-Reflecting Boundary Conditions for Maxwell's Equations*, J. Comput. Phys. **127**(1998), pp. 327-342.

43. B. Gustafsson, *The Convergence Rate for Difference Approximations to Mixed Initial Boundary Value Problems*, Math. Comp. **29**, pp. 396-406.

44. B. Gustafsson, H. O. Kreiss, and J. Oliger, *Time-Dependent Problems and Difference Methods*, John Wiley & Sons, New York, 1995.

45. T. Hagstrom, *Radiation Boundary Conditions for the Numerical Simulation of Waves*. Acta Numerica **8**(1999), pp. 47-.

46. E. Hairer, S. P. Nørsett, and G. Wanner, *Solving Ordinary Differential Equations I*. Springer Verlag, New York, 1993.

47. A. Harten, B. Engquist, S. Osher, and S. R. Chakravarthy, *Uniformly High Order Accurate Essentially Non-Oscillatory Schemes III*, J. Comput. Phys. **71**(1987), pp. 231-303.

48. J. S. Hesthaven, *A Stable Penalty Method for the Compressible Navier-Stokes Equations. III. Multi Dimensional Domain Decomposition Schemes*, SIAM J. Sci. Comp. **20**(1999), pp. 62–93.

49. J. S. Hesthaven, *From Electrostatics to Almost Optimal Nodal Sets for Polynomial Interpolation in a Simplex*, SIAM J. Numer. Anal. **35**(1998), pp. 655-676.

50. J. S. Hesthaven, *Spectral Penalty Methods*, Appl. Numer. Math. **33**(2000), pp. 23-41.

51. J. S. Hesthaven, P. G. Dinesen, and J. P. Lynov, *Spectral Collocation Time-Domain Modeling of Diffractive Optical Elements*, J. Comput. Phys. **155**(1999), pp. 287-306.

52. J. S. Hesthaven and D. Gottlieb, *Stable Spectral Methods for Conservation Laws on Triangles with Unstructured Grids*, Comput. Methods Appl. Mech. Engin. **175**(1999), pp. 361-381.

53. J. S. Hesthaven and C. H. Teng, *Stable Spectral Methods on Tetrahedral Elements*, SIAM J. Sci. Comput. **21**(2000), pp. 2352-2380.

54. J. S. Hesthaven and T. Warburton, *High-Order Nodal Methods on Unstructured Grids. I. Time-Domain Solution of Maxwell's Equations*, J. Comput. Phys. **181**(2002), pp. 1-34.

55. J. S. Hesthaven and T. Warburton, *High-Order Accurate Methods for Time-domain Electromagnetics*, Comput. Model. Engin. Sci. 2003 – to appear.

56. R. Hiptmair, *Canonical Construction of Finite Elements*, Math. Comp. **68**(1999), pp. 1325-1346.

57. R. Hiptmair, *Higher Order Whitney Forms*, Progress in Electromagnetic Research PIER **32**(2001), pp. 271-299.

58. R. Hiptmair, *Finite Elements in Computational Electromagnetics*, Acta Numerica 2002, pp. 237-339.

59. R. Holland, *Finite Difference Solutions of Maxwell's Equations in Generalized Nonorthogonal Coordinates*, IEEE Trans. Nuclear Sci. **30**(1983), pp. 4589-4591.

60. F. Q. Hu, M. Y. Hussaini, and J. L. Manthey, *Low-Dissipation and Low-Dispersion Runge-Kutta Schemes for Computational Acoustics*, J. Comput. Phys. **124**(1996), pp. 177-191.

61. F. Q. Hu, M. Y. Hussaini, and P. Rasetarinera, *An Analysis of the Discontinuous Galerkin Method for Wave Problems*, J. Comput. Phys. **151**(1999), pp. 921-946.

62. F. Q. Hu and H. L. Atkins, Eigensolution Analysis of the Discontinuous Galerkin Method with Non-Uniform Grids, Part I: One Space Dimension, ICASE Report No. 2001-40, 2001.

63. T. J. R. Hughes, *The Finite Element Method: Linear and Dynamic Finite Element Analysis*. Dover Publications, New York, 2000.

64. B.-N. Jiang, *Least Squares Finite Element Methods: Theory and Applications in Computational Fluid Dynamics and Electromagnetics*. Springer-Verlag, New York, 1998.

65. B.-N. Jiang, J. Wu, and L.A. Povinelli, *The Origin of Spurious Solutions in Computational Electromagnetics*, J. Comput. Phys. **125**(1996), pp. 104-123.

66. D. Jiao and J. M. Jin, *Three-Dimensional Orthogonal Vector Basis Functions for Time-Domain Finite Element Solution of Vector Wave Equations*, IEEE Trans. Antennas Propagat. – to appear 2001.

67. D. Jiao, J. M. Jin, E. Michielssen, and D. Riley, *Time-Domain Finite-Element Simulation of Three-Dimensional Scattering and Radiation Problems using Perfectly Matched Layers*, IEEE Trans. Antennas Propagat. – to appear 2001.

68. D. Jiao, A. Ergin, B. Shanker, E. Michielssen, and J. M. Jin, *A Fast Time-Domain Higher-Order Finite-Element Boundary-Integral Method for 3-D Electromagnetic Scattering Analysis*, IEEE Trans. Antennas Propagat. – to appear 2002.

69. J. M. Jin, *The Finite Element Method in Electromagnetics*. John Wiley & Sons, Inc. 1993.

70. T.G. Jurgens, A. Taflove, K. Umashaankar, and T.G. Moore, *Finite-Difference Time-Domain Modeling of Curved Surfaces*, IEEE Trans. Antennas Propaga. **40**(1992), pp. 357-366.

71. A. Kabakian, *A Spectral Algorithm for Electromagnetic Wave Scattering in the Time Domain – Applications to RCS Computations*, AIAA Paper 96-2334, 1996.

72. U. Kangro and R.A. Nicolaides, *Spurious Fields in Time-Domain Computations of Scattering Problems*, IEEE Trans. Antennas Propagat. **45**(1997), pp. 228-234.

73. G. E. Karniadakis and S. J. Sherwin, *Spectral/hp Element Methods for CFD*. Numerical Mathematics and Scientific Computation. Clarendon Press, Oxford. 1999.

74. C. A. Kennedy and M. H. Carpenter, *Additive Runge-Kutta Schemes for Convection-Diffusion-Reaction Equations*, Appl. Numer. Math. 2002 – to appear.

75. T. Koornwinder, *Two-variable Analogues of the Classical Orthogonal Polynomials* in "Theory and Application of Special Functions", R.A. Askey ed., Academic Press, 1975. pp. 435-495.

76. D. A. Kopriva, *A Spectral Multidomain Method for the Solution of Hyperbolic Systems*, Appl. Numer. Math. **2**(1986), pp. 221-241.

77. D. A. Kopriva, *Computation of Hyperbolic Equations on Complicated Domains with Patched and Overset Chebyshev Grids*, SIAM J. Sci. Stat. Comput. **10**(1989), pp. 120-132.

78. D. A. Kopriva, S. L. Woodruff, and M. Y. Hussaini, *Discontinuous Spectral Element Approximation of Maxwell's Equations*. In Discontinuous Galerkin Methods: Theory, Computation and Applications. B. Cockburn, G. E. Karniadakis, and C.W. Shu (Eds). Lecture Notes in Computational Science and Engineering **11**(2000), Springer Verlag, New York. pp. 355-362.

79. D. A. Kopriva, S. L. Woodruff, and M. Y. Hussaini, *Computation of Electromagnetic Scattering with a Non-Conforming Discontinuous Spectral Element Method*, Int. J. Num. Meth. Engin. **53**(2002), pp. 105-122.

80. H. O. Kreiss and J. Oliger, *Comparison of Accurate Methods for the Integration of Hyperbolic Problems*, Tellus **24**(1972), pp. 199-215.

81. H.O. Kreiss and G. Scherer, *Finite Element and Finite Difference Methods for Hyperbolic Partial Differential Equations*. In Mathematical Aspects of Finite Elements in Partial Differential Equations. Academic Press, NY, 1974.

82. J. F. Lee, R. Lee, and A. Cangellaris, *Time-Domain Finite-Element Methods*, IEEE Trans. Antennas Propagat. **45**(1997), pp. 430-441.

83. J. F. Lee and R. Lee (Eds), *Special Issue on Computational Electromagnetics*, Comput. Methods Appl. Mech. Engrg. **169**(1999).

84. S. K. Lele, *Compact Finite-Difference Schemes with Spectral-Like Resolution*, J. Comput. Phys. **103**(1992), pp. 16-42.

85. Q. Li, Y. Chen and D. Ge, *Comparison Study of the PSTD and FDTD Methods for Scattering Analysis*, Microwave Opt. Techno. Lett. **25**(2000), pp. 220-226.

86. Q.H. Liu, *The PSTD Algorithm: A Time-Domain Method Requiring only Two Cells Per Wavelength*, Microwave Opt. Techno. Lett. **15**(1997), pp. 158-165.

87. Q. H. Liu, *Large-Scale Simulations of Electromagnetic and Acoustic Measurements Using the Pseudospectral Time-Domain (PSTD) Algorithm*, IEEE Trans. Geosci. Remote Sensing **37**(1999), pp. 917-926.

88. D. R. Lynch and K. D. Paulsen, *Time-Domain Integration of the Maxwell Equations on Finite Elements*, IEEE Trans. Antennas Propagat. **38**(1990), pp. 1933-1942.

89. D. R. Lynch and K. D. Paulsen, *Origin of Vector Parasites in Numerical Maxwell Solutions*, IEEE Trans. Microwave Theo. Techniq. **39**(1991), pp. 383-394.

90. A. H. Mohammadian, V. Shankar, and W. F. Hall, *Computation of Electromagnetic Scattering and Radiation using a Time-Domain Finite-Volume Discretization Procedure*, Comput. Phys. Comm. **68**(1991), pp. 175-196.

91. P. Monk and E. Suli, *Error Estimates of Yee's Method on Non-Uniform Grids*, IEEE Trans. Magnetics **30**(1994), pp. 393-412.

92. A. Nachman, *MINIREVIEW: A Brief Perspective on Computational Electromagnetics*, J. Comput. Phys. **126**(1996), pp. 237-239.

93. J. C. Nedelec, *Mixed Finite Elements in R^3*, Numer. Math. **35**(1980), pp. 315-341.

94. J. C. Nedelec, *A New Family of Mixed Finite Elements in R^3*, Numer. Math. **50**(1986), pp. 57-81.

95. J. Nordström and R. Gustafsson, *High-Order Finite Difference Approximations of Electromagnetic Wave Propagation Close to Material Discontinuities*, J. Sci. Comput. 2002 – to appear.

96. P. Olsson, *Summations by Parts, Projections, and Stability I*, Math. Comp. **64**(1995), pp. 1035-1065.

97. P. Olsson, *Summations by Parts, Projections, and Stability II*, Math. Comp. **64**(1995), pp. 1473-1493.

98. K. D. Paulsen and D. R. Lynch, *Elimination of Vector Parasites in Finite Element Maxwell Solutions*, IEEE Trans. Microwave Theo. Techniq. **39**(1991), pp. 395-404.

99. K. D. Paulsen, W. E. Boyse, and D. R. Lynch, *Continuous Potential Maxwell Solutions on Nodal-Based Finite Elements*, IEEE Trans. Antennas Propagat. **40**(1992), pp. 1192-1200.

100. P. G. Petropoulous, *Phase Error Control for FD-TD Methods of Second and Fourth Order Accuracy*, IEEE Trans. Anten. Prop. **42**(1994), pp. 859–862.

101. P.G. Petropoulos, L. Zhao, and A.C. Cangellaris, *A Reflectionless Sponge Layer Absorbing Boundary Condition for the Solution of Maxwell's Equations with High-Order Staggered Finite Difference Schemes*, J. Comput. Phys. **139**(1998), pp. 184-208.

102. P. G. Petropoulos and A. Yefet, *Subgridding a Fourth-Order FD-TD Scheme for Maxwell's Equations*. In Proceedings of Fourth International Workshop on Computational Electromagnetics in the Time-Domain: TLM/FDTD and Related Techniques (CEM-TD). C. Christopoulos (Eds), Nottingham, UK, 2001. p. 39-45.

103. J. Proriol, *Sur une Famille de Polynomes à deux Variables Orthogonaux dans un Triangle*, C. R. Acad. Sci. Paris **257**(1957), pp. 2459-2461.

104. K. R. Rao, J. Nehrbass, and R. Lee, *Discretization Errors in Finite Methods: Issues and Possible Solutions*, Comput. Methods Appl. Mech. Engrg. **169**(1999), pp. 219-236.

105. V. S. Ryaben'kii, S. V. Tsynkov, and V. I. Turchaninov, *Global Discrete Artificial Boundary Condition for Time-Dependent Wave Propagation*, J. Comput. Phys. **174**(2001), pp. 712-758.

106. J. S. Shang, *High-Order Compact Difference Schemes for Time-Dependent Maxwell Equations*, J. Comput. Phys. **153**(1999), pp. 312-333.

107. J. S. Shang and R. M. Fithen, *A Comparative Study of Characteristic Based Algorithms for the Maxwell's Equations*, J. Comput. Phys. **125**(1996), pp. 378-394.

108. J. S. Shang and D. Gaitonde, *Characteristic-Based Time-Dependent Maxwell Equation Solvers on a General Curvilinear Frame*, AIAA J. **33**(1995), pp. 491-498.

109. J. S. Shang and D. Gaitonde, *On High-Resolution Schemes for Time-Dependent Maxwell Equations*, AIAA Paper 96-0832, 34th Aerospace Sciences Meeting & Exhibit, Reno, NV, 1996.

110. J. S. Shang, D. Gaitonde, and K. Wurtzler, *Scattering Simulations of Computational Electromagnetics*, AIAA Paper 96-2337, 34th Aerospace Sciences Meeting & Exhibit, Reno, NV, 1996.

111. P. Silvester, *Finite Element Solution of Homogeneous Waveguide Problems*, Alta Frequenza **38**(1969), pp. 313-317.

112. P. P. Silvester and R. L. Ferrari, *Finite Elements for Electrical Engineers*. Cambridge University Press, Cambridge, UK. 1983.

113. B. Strand, *Summation by Parts for Finite Difference Approximations of d/dx*, J. Comput. Phys. **110**(1994), pp. 47-67.

114. G. Strang, *Accurate Partial Difference Methods II. Non-linear Problems*, Numer. Math. **6**(1964), pp. 37-46.

115. D. Sun, J. Manges, X. Yuan, and Z. Cendes, *Spurious Modes in Finite Element Methods*, IEEE Antennas Propagat. Mag. **37**(1995), pp. 12-24.

116. A. Taflove, *Computational Electrodynamics - The Finite-Difference Time-Domain Method*, Aztech House, Boston, 1995.

117. A. Taflove (Eds.), *Advances in Computational Electrodynamics: The Finite-Difference Time-Domain Method*, Aztech House, Boston, 1998.

118. C. K. W. Tam and J. C. Webb, *Dispersion-Relation-Preserving Finite Difference Schemes for Computational Acoustics*, J. Comput. Phys. **107**(1993), pp. 262-281.

119. E. Turkel and A. Yefet, *On the Construction of a High-Order Difference Scheme for Complex Domains in a Cartesian Grid*, Appl. Numer. Math. **33**(2000), pp. 113-124.

120. J.L. Volakis, A. Chatterjee and L. Kempel, *Finite Element Methods for Electromagnetics: Antennas, Microwave Circuits and Scattering Applications*. IEEE Press, 1998.

121. S. Wang, F. L. Teixeria, R. Lee, and J.-F. Lee, *DRP Schemes for Electrically Large 2D FDTD Simulations*, IEEE Trans. Antennas Propagat. 2001 – submitted.

122. S. Wang, F. L. Teixeria, R. Lee, and J.-F. Lee, *Dispersion-Relation-Preserving FDTD Algorithms for Large Scale Three-Dimensional Problems*, IEEE Trans. Antennas Propagat. 2002 – submitted.

123. T. Warburton, *Application of the Discontinuous Galerkin Method to Maxwell's Equations Using Unstructured Polymorphic hp-finite Elements*. In Discontinuous Galerkin Methods: Theory, Computation and Applications. B. Cockburn, G. E. Karniadakis, and C.W. Shu (Eds). Lecture Notes in Computational Science and Engineering **11**(2000), Springer Verlag, New York. pp. 451-458.

124. C. E. Wasberg and D. Gottlieb, *Optimal Strategy in Domain Decomposition Spectral Methods for Wave-Like Phenomena*, SIAM J. Sci. Comput. **22**(2000), pp. 617-632.

125. J. P. Webb, *Hierarchal Vector Basis Functions of Arbitrary Order for Triangular and Tetrahedral Finite Elements*, IEEE Trans. Antennas Propagat. **47**(1999), pp. 1244-1253.

126. Z. Xie, C.-H. Chan, and B. Zhang, *An Explicit Fourth-Order Orthogonal Curvilinear Staggered-Grid FDTD Method for Maxwell's Equations*, J. Comput. Phys. **175**(2002), pp. 739-763.

127. B. Yang and D. Gottlieb, *Comparisons of Staggered and Non-Staggered Schemes for Maxwell's Equations*. In Proceedings of the 12'th Annual Review of Progress in Applied Computational Electromagnetics, Naval Postgraduate School, Monterey, CA, March 1996, vol. II, pp. 1122–1131.

128. B. Yang, D. Gottlieb, and J. S. Hesthaven, *On the Use of PML ABC's in Spectral Time-Domain Simulations of Electromagnetic Scattering*. Proc. of The 13'th Annual Review of Progress in Applied Computational Electromagnetics, Monterey, CA. 926-933, 1997.

129. B. Yang, D. Gottlieb, and J. S. Hesthaven, *Spectral Simulations of Electromagnetic Wave Scattering*, J. Comput. Phys. **134**(1997), pp. 216-230.

130. B. Yang and J. S. Hesthaven, *A Pseudospectral Method for Time-Domain Computation of Electromagnetic Scattering by Bodies of Revolution*, IEEE Trans. Antennas Propaga. **47**(1999), pp. 132-141.

131. B. Yang and J. S. Hesthaven, *Multidomain Pseudospectral Computation of Maxwell's Equations in 3-D General Curvilinear Coordinates*, Appl. Numer. Math. **33**(2000), pp. 281-289.

132. K. S. Yee, *Numerical Solution of Initial Boundary Value Problems Involving Maxwell's in Isotropic Media*, IEEE Trans. Antennas Propagation **14**(1966), pp. 302-307.

133. K. S. Yee, J. S. Chen, and A. H. Chang, *Conformal Finite-Difference Time-Domain (FDTD) with Overlapping Grids*, IEEE Trans. Antennas Propag. **40**(1992), pp. 1068-1075.

134. A. Yefet and P.G. Petropoulos, *A Staggered Fourth-Order Accurate Explicit Finite Difference Scheme for the Time-Domain Maxwell's Equations*, J. Comput. Phys. **168**(2001), pp. 286-315.

135. A. Yefet and E. Turkel, *Fourth-Order Compact Implicit Method for the Maxwell Equations with Discontinuous Coefficients*, Appl. Numer. Math. **33**(2000), pp. 125-134.

136. C. Zhang and W.W. Symes, *Fourth Order Methods for Acoustic Waves with Discontinuous Material*, in Proc of 4th International Conference on Mathematical and Numerical Aspects of Wave Propagation, J. deSantos et al. (Eds), Philadelphia, 1998.

137. C. Zhang and W.W. Symes, *Fourth Order, Full Stencil Immersed Interface Method for Elastic Waves with Discontinuous Material*, in Proc of 4th International Conference on Mathematical and Numerical Aspects of Wave Propagation, J. deSantos et al. (Eds), Philadelphia, 1998.

138. G. Zhao and Q. H. Liu, *The 2.5-D Multidomain Pseudospectral Time-Domain Algorithm*, IEEE Trans. Antennas Propagat. – to appear 2002.

139. G. Zhao, Y. Q. Zeng, and Q. H. Liu, *The 3-D Multidomain Pseudospectral Time-Domain Method*, IEEE Trans. Antennas Propagat. – submitted 2002.